AD-A166 662 EFFECTS OF PLANFORM GEOMETRY ON HOVER PERFORMANCE OF A 2-METER-DIAMETER M... (U) NATIONAL AERONAUTICS AND SPACE ADMINISTRATION HAMPTON VA LANG... A E PHELPS ET AL. 1/1

UNCLASSIFIED MAR 86 NASA-L-16020 NASA-TM-87607 F/G 20/4 NL

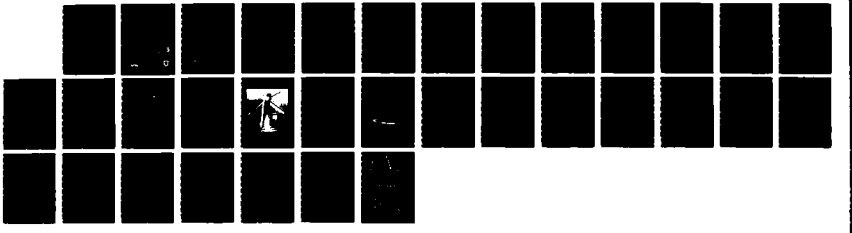

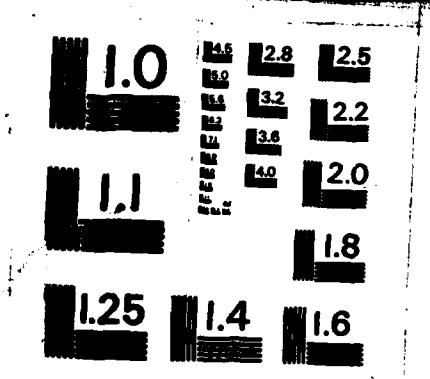

AD-A166 662

DTIC FILE COPY

DTIC
ELECTE
APR 17 1986
A

This document has been approved for public release and sale; its distribution is unlimited

86 4 10 034

NASA
Technical Memorandum 87607

AVSCOM
Technical Report 85-B-6

Effects of Planform Geometry on Hover Performance of a 2-Meter-Diameter Model of a Four-Bladed Rotor

Arthur E. Phelps III and Susan L. Althoff
Aerostructures Directorate
USAARTA-AVSCOM
Langley Research Center
Hampton, Virginia

National Aeronautics
and Space Administration
Scientific and Technical
Information Branch
1986

Summary

Hover tests of three different four-bladed rotors were conducted using a small-scale rotor model equipped with a fully articulated hub. Tests were conducted on a swept-tip baseline configuration with a rectangular planform, a configuration with a 3-to-1 taper over the outboard 20 percent of the blade span (TR3), and a configuration with a 5-to-1 taper over the outboard 20 percent of the blade span (TR5). The investigation covered a range of tip speeds and thrust coefficients. The two tapered configurations had better hover performance than the baseline configuration, and the TR3 configuration was somewhat better than the TR5 configuration above a rotor thrust coefficient of 0.004. The test results were compared with predictions made by using a prescribed-wake analysis, a momentum strip-theory analysis, and a simplified free-wake analysis. The performance of the baseline blade was in fair agreement with predictions from both the momentum strip-theory analysis and the prescribed-wake analysis when appropriate low Reynolds number airfoil data were used. The performance of the two tapered-blade configurations was in fair agreement with the predictions of the momentum strip-theory analysis; however, the prescribed-wake analysis predicted performance that was much worse than measured for the two tapered configurations.

Introduction

A factor of major importance in the design and development of a new helicopter is the ability to predict accurately the hovering performance of the rotor. This ability is becoming a more important and challenging task as the development of new materials and fabrication techniques allows the construction of blades with complex geometries involving different airfoils, planform variations, and nonlinear twist distributions. Among the analytic tools available to the designer, the prescribed-wake analysis has proven to be a powerful, accurate, and relatively inexpensive method of evaluating the hovering performance of rotors. (See refs. 1 to 6.) The prescribed-wake analysis is a semi-empirical procedure in which an experimental data base is used to establish a geometric and aerodynamic definition of the wake structure from a thrusting rotor. The performance of the rotor is then evaluated in terms of the resulting wake geometry. The sensitivity of these types of analyses to the wake geometry was illustrated in reference 1, where a change in tip-vortex position of 0.5 percent of the rotor radius resulted in a thrust change of nearly 3 percent.

The data base upon which many current versions of the prescribed-wake method rely consists almost entirely of data acquired from blades with a rectangular planform. Both twist and planform are known to have a primary influence on the structure of the wake, particularly with respect to the strength and location of the tip vortex. While the effects of twist distribution have been included in current versions of the prescribed-wake analysis, the effects of blade-planform variation are not in the public domain. The analysis method has been shown to be quite good at predicting the performance of rotors with rectangular blades, but it is very sensitive to small changes in wake geometry. Considering the impact that blade planform is known to have on the behavior of the tip vortex, it is timely to reconsider the suitability of using prescribed-wake analyses in their present form for predicting the hover performance of rotors with nonrectangular blade planforms.

The present investigation was conducted primarily to provide some exploratory experimental data for comparison with analysis concerning the effect of blade-planform taper on hover performance. The experiments consisted of measuring the thrust and torque characteristics of four-bladed, fully articulated rotors with three different blade planforms: a swept-tip rectangular planform, a planform with a 3-to-1 taper ratio over the outboard 20 percent of the blade, and a planform with a 5-to-1 taper ratio over the outboard 20 percent of the blade. Data for each of the three configurations were obtained over a range of thrust coefficients from approximately 0 to 0.0075 and for a range of tip speeds from 300 to 600 ft/sec. As a secondary effort, the experimental data were compared with predictions made by the prescribed-wake analysis described in reference 1, a strip-theory momentum analysis based primarily on the equations of reference 7, and the simplified free-wake analysis described in reference 8.

Symbols

Data in this report are presented in coefficient form and are referenced to the shaft-axis system shown in figure 1.

$C_{L,\max}$	maximum lift of airfoil section
$\partial C_L/\partial\alpha$	lift-curve slope of airfoil section
C_Q	rotor torque coefficient, $M_Z/\rho\pi R^3(\Omega R)^2$
C_T	rotor thrust coefficient, $T/\rho\pi R^2(\Omega R)^2$
c	local blade chord, in.
c_e	thrust-weighted equivalent blade chord, $\int_0^1 cx^3\,dx/\int_0^1 x^3\,dx$, in.

c_{tip}	rotor tip chord, in.
D	rotor drag force, lbf
FM	rotor figure of merit, $C_T^{3/2}/C_Q\sqrt{2}$
L	rotor lift force, lbf
M_Z	rotor torque, in-lbf
N_{Re}	Reynolds number, Vc/ν
$N_{Re,tip}$	rotor tip Reynolds number, $V_{tip}c_{tip}/\nu$
R	rotor radius, in.
r	radial distance along blade, in.
T	rotor thrust, $\sqrt{L^2+D^2+Y^2}$, lbf
TR3	blade planform with a 3-to-1 taper ratio
TR5	blade planform with a 5-to-1 taper ratio
V	local velocity, ft/sec
V_{tip}	rotor tip speed, ft/sec
x, y, z	Cartesian coordinates
x	nondimensional blade radius, r/R
Y	rotor side force, lbf
ν	kinematic viscosity of air, ft^2/sec
ρ	atmospheric density, $slugs/ft^3$
σ_T	thrust-weighted solidity, $4c_e/\pi R$
Ω	rotor rotational speed, rad/sec

Model and Equipment

The model used in the investigation is shown schematically in figure 2(a) and is a general-research model known as the 2-meter rotor test system (2MRTS). The model is shown in figure 2(b) mounted for testing in a static test area of the Langley 4- by 7-Meter Tunnel. The 2MRTS has a 29-horsepower, three-phase, variable-frequency electric motor and is equipped with a four-bladed, fully articulated hub onto which the rotor blades are mounted. Basically, the 2MRTS is a rotor power and control package on which a fuselage model of a particular helicopter being studied may be mounted and is essentially independent of the helicopter external configuration. For the present tests, a general-research fuselage was used, and the different rotor configurations used in the tests were obtained by changing the rotor blades on the hub.

The fiberglass fuselage shown in the figure is a hybrid design which is generally representative of configurations in common use, but it is not a model of any specific helicopter. The body contours were completely defined by a closed-form mathematical expression, so that the fuselage could be modeled easily for use in computational aerodynamic analyses. A complete definition of the body mathematical model, including a description of the modeling procedure, is presented in reference 9, and significant details of the procedure are given in the appendix, which is taken from reference 9.

The 2MRTS has provisions for mounting the fuselage on its own independent balance, but a suitable balance was not available for use at the time the tests were conducted. The rotor balance measurements for the present investigation therefore include a presently undefined contribution as the result of mutual interference effects between the body and the rotor.

Tests were conducted using the three blade planforms described in figures 3(a) and 3(b). The model blade structure is shown in figure 3(c). The geometry of the baseline swept-tip blade was based on the planform and twist distribution of the Sikorsky UH-60A Black Hawk helicopter, primarily because the Black Hawk is representative of current rotor technology. The two tapered-blade configurations were designed as general-research rotors for this test and are designated as TR3 and TR5. The blades were designed by using a strip-theory hover momentum analysis developed by the U.S. Army Aerostructures Directorate (AVSCOM) and the forward-flight performance analysis of reference 10. Thrust-weighted solidity was 0.0825 for all three rotors. Because of the secondary influences of airfoil section on radial circulation distribution, and in order to simplify fabrication, the NACA 0012 airfoil section was used for all blades.

No attempt was made to model any specific blade dynamic properties or to evaluate the effects of aeroelasticity. The model blades were designed to have conservative strength and fatigue margins for general-research investigations in both hover and forward flight, and the aeroelastic properties of the blades were designed to ensure that there would be no coalescence of fundamental blade frequencies with integer multiples of the rotor frequencies over the normal operating range of the 2MRTS. The resulting blades are somewhat heavy when compared with Mach scaled, dynamically similar subscale blades of full-scale helicopters, but are very stiff torsionally and are very durable for use in the severe environments often encountered in general-research studies.

Tests and Procedures

Tests were conducted with the model mounted in the static model preparation area (MPA) of the Langley 4- by 7-Meter Tunnel. (See fig. 4.) The

MPA is a large, open room with a floor-to-ceiling height of 35 ft and is used regularly as a closed test cell for model jet-engine simulation, propeller static testing, and rotor hover testing. The model was mounted on a strut with the rotor shaft vertical and with the hub plane of rotation located 1.14 rotor diameters above the floor. (See fig. 4.) Smoke flow visualization was used to verify that there was no significant wake reingestion over the range of parameters investigated.

Tests were run by first setting rotor rotational speed to obtain the desired tip speed and then varying the collective pitch to provide a range of thrust from near zero to the maximum thrust available from the system. A run was terminated when motor temperatures indicated that the motor was at its maximum power output. Tests were conducted over a range of thrust coefficients from approximately 0 to 0.0075 and over a range of tip speeds from 300 to 600 ft/sec for each configuration.

The repeatability of the data was checked frequently during the test program and was found to be good. The accuracy of the measurements was determined by the balance sensitivity. Thrust coefficient C_T was accurate within $\pm 6.7 \times 10^{-6}$, torque coefficient C_Q was accurate within $\pm 5.0 \times 10^{-6}$, and figure of merit FM was accurate within $\pm 2.4 \times 10^{-3}$.

Presentation of Results

Experimental results are presented in both tabular and graphical form, and comparisons of the test data with the analytic predictions are presented graphically. Numerical values of tip speed, thrust and torque coefficients, and figure of merit are presented in tables I, II, and III for the baseline, TR3, and TR5 configurations, respectively. Plots of data in coefficient form are presented as follows:

Results and Discussion

The results of the experiments are presented in figures 5(a) to 5(c) as torque coefficient C_Q and figure of merit FM plotted against thrust coefficient C_T for all three rotors, and comparisons between the planforms are shown in figures 6 and 7. Rotor performance improvement is defined as a decrease in required torque and an increase in efficiency for a given thrust value. The data of figure 5 are presented for a range of tip speeds to provide some indication of the effect of Reynolds number on the hover performance of the rotors. The data of figure 5(a) show that the effect of tip speed on the performance of the baseline blade was evident primarily at the higher thrust coefficients. At $C_T = 0.005$, for example, figure of merit varied from 0.59 at $V_{tip} = 300$ ft/sec to 0.61 at $V_{tip} = 600$ ft/sec. For values of C_T below about 0.004, the largest increment in FM was only about 0.01. The torque-required curves show that the baseline rotor required slightly more power for a given value of C_T at $V_{tip} = 300$ ft/sec than was the case for higher tip speeds, but the increments due to tip-speed variations were generally quite small. Unfortunately, the 2MRTS was power limited for the baseline rotor; as a result, values of C_T greater than 0.0062 could not be obtained, so a maximum FM was not determined.

The performance of the rotor with the TR3 planform is shown in figure 5(b). There was a significant impact of tip speed on performance as V_{tip} was increased from 300 to 400 ft/sec, but above $V_{tip} = 400$ ft/sec the effect of tip speed was much less dramatic. Between $C_T = 0.0040$ and 0.0050, there was a noticeable dip in the FM curves for all tip speeds tested. It is possible that a portion of the blade experienced partial flow separation, but detailed flow studies were not conducted. The break is not easily discernible in the torque curves, so the phenomenon responsible for the trend is apparently related more to lift than to drag, although the available data are inadequate to establish the cause precisely. Increasing tip speed from 400 to 600 ft/sec resulted in a small increase in FM for $C_T > 0.004$ and caused a slight reduction in power required.

The performance data of figure 5(c) for the rotor with the TR5 planform do not show the dramatic effect of tip speed seen with the TR3 planform. Instead, there was a gradual increase in FM and a gradual reduction in torque required as the tip speed was increased from 300 to 500 ft/sec. There was almost no change in performance as tip speed was further increased to 600 ft/sec. There were two areas on the FM curve where there was a noticeable slope change: one at $C_T \approx 0.0026$ and another at $C_T \approx 0.0047$. There was not an abrupt change in slope at these points, but rather there was a noticeable change over a fairly small increment in C_T, suggesting a localized flow separation somewhere along the blade. As was the case with the TR3 planform data, the

slope changes on the FM curve were difficult to detect on the torque-required curves.

The performances of the three rotors are compared in figures 6(a) and 6(b) for tip speeds of 300 and 600 ft/sec, respectively. The data of figure 6(a) at $V_{tip} = 300$ ft/sec indicate that the baseline and TR3 planforms had essentially the same performance, and both were inferior to the TR5 planform at this low tip speed. The superiority of the TR5 planform began to emerge gradually as C_T was increased and was easily seen for values of C_T greater than about 0.004. At a tip speed of 600 ft/sec, the characteristics were quite different, however, as can be seen in figure 6(b). For thrust coefficients greater than 0.0025, the data show that both the tapered planforms had better performance than did the baseline planform. The data for the tapered blades do, however, contain an unexpected variation between the two planforms. Below $C_T = 0.004$, the figure of merit for the TR5 planform was higher than for the TR3 planform; for $C_T > 0.004$, the TR3 planform had the higher figure of merit.

The crossover in figure of merit for the tapered blades can be understood by considering at least two possibilities. First, the smaller tip chord, and therefore Reynolds number, for the TR5 blades may have caused the tip sections of the TR5 blade to stall at lower angles of attack than the tips of the TR3 blades. At higher thrust coefficients where the blade was operating at a high angle of attack, the reduced stall angles for the TR5 blades would be manifested as reduced FM and higher torque for a given level of thrust. A second possibility is that the reduced tip chord of the TR5 blade would produce a weaker tip vortex with reduced downwash velocity, thereby causing the TR5 tip vortex to have a greater influence on the lift of the following blade than was the case for the TR3 configuration. Of course, a combination of the two factors could also affect the results.

Figure 7 is a comparison of the characteristics of the TR3 and TR5 planforms for approximately the same tip Reynolds number obtained by operating the TR3 planform at a tip speed of 400 ft/sec and the TR5 planform at 650 ft/sec. The data show that the TR5 blade had slightly better performance than the TR3 blade for $C_T < 0.0047$, but the TR3 blade was slightly better for $C_T > 0.0047$. The TR5 blade had a figure of merit of 0.66 at $C_T = 0.0065$, and the relatively flat slope of the FM curve at that point suggests that the TR5 blade had nearly reached its peak performance. The maximum measured figure of merit for the TR3 blade, however, was 0.70 at $C_T = 0.0074$, and the positive slope of the curve at that point suggests that some additional increases in FM could be expected if the thrust coefficient were increased. Since the tip Reynolds number for both blades was the same in figure 7, the Reynolds numbers inboard of the taper were approximately 38 percent lower for the TR3 planform than for the TR5 planform. Also, since the effects of decreased Reynolds number are generally seen as reduced $\partial C_L/\partial\alpha$ and $C_{L,\max}$, the TR3 planform was operating at an aerodynamic disadvantage compared with the TR5 blade. If the primary factor influencing the crossover in the FM and torque-required curves for the tapered blades in figure 6(b) were Reynolds number, it would be reasonable to expect the FM curve for the TR3 planform in figure 7 to lie below the curve for the TR5 planform. Since that was not the case, it appears that the location of the tip vortex was the dominant factor affecting the crossover point noted in figure 6(b), and the influence of Reynolds number was of secondary importance for this comparison.

Figure 8 is a comparison of the test data with predictions based on analysis for each of the three rotors for experimental data obtained at 600 ft/sec. As noted previously, three different methods reflecting fundamentally different formulations were used in the predictions: a prescribed-wake analysis from reference 1, a momentum analysis based on the equations of reference 7, and a free-wake analysis from reference 8. The prescribed-wake method used a lifting-line analysis to calculate a nonuniform inflow distribution. Hover performance was then determined by strip theory and two-dimensional airfoil data. The momentum method used a strip analysis with a nonuniform inflow velocity distribution based on blade-segment lift coefficient and included a linear lift-loss factor over the outboard 5 percent of the blade. The simplified free-wake analysis modeled the wake with vortex lines and calculated rotor performance using strip theory and a lifting-line representation of the blade. These particular analyses were chosen for use because they are comparatively inexpensive to execute, they are typical of the type of preliminary analyses which might be used to conduct an evaluation of a number of candidate rotors for a particular specification, and they are generally representative of the analytic codes available to the designer or researcher from the open literature. The curves shown in figure 8 are a least-squares fit of the computed coefficients. The predicted performance for the baseline planform is shown in figure 8(a), and the predictions for the TR3 and TR5 blades are shown in figures 8(b) and 8(c), respectively. The figures show that the prescribed-wake analysis predicted better than measured performance for the baseline blade and worse than measured performance for both tapered blades. The momentum and free-wake analy-

ses both predicted better than measured performance for all three blade configurations. The poor performance predicted by the prescribed-wake analysis for the tapered blades is considered by the authors to be mainly the result of improper coupling of the empirical wake structure with the actual radial lift distribution on the tapered blade. The generalized wake model used in the code is based on data obtained from rectangular blades, and the effects of taper have not been quantified as to their impact on the generalized structure, particularly with respect to the tip-vortex path.

The better than measured performance prediction for the baseline blade is primarily the result of Reynolds number effects on the airfoil aerodynamic characteristics. (See fig. 9.) The predictions shown in figure 9 were obtained by using both high and low Reynolds number airfoil data sets (ref. 11) in each of the prescribed-wake and momentum analyses. Reynolds number effects on the simplified free-wake analysis were not addressed because there was no provision for modeling either the planform or the viscous-drag characteristics of the airfoil. One set of airfoil data used in the analyses was obtained at Reynolds numbers representative of full-scale flight; the other set of data was obtained at Reynolds numbers representative of model blades with a chord of about 4 in. The Reynolds numbers for the test blades at a tip speed of 600 ft/sec are lower than those for either of the available data sets, as reflected by the model blade chords shown in figure 3(a). The overall effect of reduced Reynolds number in the analyses was to reduce the rotor performance by causing an increase in torque required for a given value of thrust. That trend resulted in a much worse than measured performance prediction for the tapered blades based on the prescribed-wake analysis but brought the predictions based on momentum analysis into better agreement with the test results shown in figures 9(b) and 9(c).

Summary of Results

Hover tests of three different four-bladed rotors were conducted using a small-scale rotor model equipped with a fully articulated hub. Tests were conducted on a swept-tip baseline configuration with a rectangular planform, a configuration with a 3-to-1 taper over the outboard 20 percent of the blade span (TR3), and a configuration with a 5-to-1 taper over the outboard 20 percent of the blade span (TR5). The investigation covered a range of tip speeds and thrust coefficients, and the results were compared with predictions made by using a prescribed-wake analysis, a momentum strip-theory analysis, and a simplified free-wake analysis. The results of the investigation and comparison with analyses are briefly summarized as follows:

1. The tapered TR3 and TR5 configurations had generally better hover performance than did the baseline rectangular configuration.
2. For the two tapered configurations at the higher tip speeds, the TR5 blade had slightly better performance at a rotor thrust coefficient C_T of less than 0.004, but the TR3 blade had better performance for $C_T > 0.004$.
3. The performance of the baseline configuration was in fair agreement with predictions, based on the prescribed-wake and momentum analyses, when the deleterious effects of low Reynolds number were included in the analysis.
4. The performance of the two tapered configurations was in fair agreement with predictions based on the momentum strip theory when appropriate Reynolds number data were used, but the measured performance was much better than the performance predicted by the prescribed-wake analysis used in the present study.
5. Performance predictions based on the simplified free-wake analysis used herein were generally much better than those measured in the experiments for all three planform configurations.

NASA Langley Research Center
Hampton, VA 23665-5225
November 26, 1985

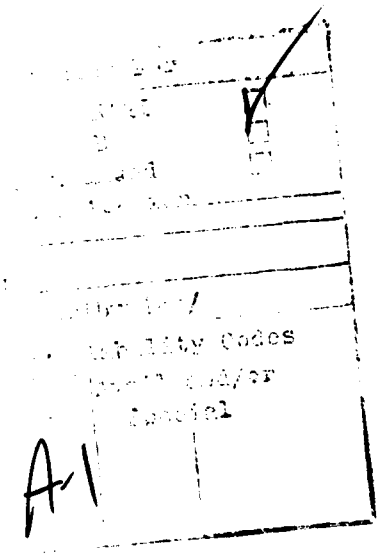

Appendix

Description of Fuselage Used In Tests[1]

The fuselage contours used on the generalized body were chosen so that they could be described by a simple mathematical formulation, thereby easing the problem of numerical modeling of the body for use in computational aerodynamic evaluation of experimental studies. The fuselage shape was developed in reference 9 and is derived from super-ellipse equations where, for a given fuselage station X, the cross section (Y- and Z-coordinates) is defined by the height H, width W, camber line $Z0$, and elliptical power N.

A super ellipse is defined by the elliptical equation

$$\left(\frac{x+x0}{A}\right)^n + \left(\frac{y+y0}{B}\right)^m = C \qquad \text{(A1)}$$

where n and m are not necessarily equal to two or equal to each other, and where A, B, C, $x0$, and $y0$ are arbitrary constants. By solving for y as a function of x (i.e., $y = F(x)$), equation (A1) becomes

$$y = F(x) = B\left[C - \left(\frac{x+x0}{A}\right)^n\right]^{1/m} - y0 \qquad \text{(A2)}$$

By making the substitutions $m = C_8$; $y0 = -C_6$; $B = C_7$; $C = C_1$; and $X = x$ and by expanding the term

$$-\left(\frac{x+x0}{A}\right)^n \qquad \text{(A3)}$$

to

$$+C_2\left(\frac{X+C_3}{C_4}\right)^{C_5} \qquad \text{(A4)}$$

Equation (A2) becomes

$$F(X) = C_6 + C_7\left[C_1 + C_2\left(\frac{X+C_3}{C_4}\right)^{C_5}\right]^{1/C_8} \qquad \text{(A5)}$$

Equation (A5) is then used to calculate H, W, $Z0$, and N as a function of X by selection of an appropriate set of constants C_1 through C_8. (See table A1.)

The cross section at fuselage station X can then be defined by a polar coordinate (r, ϕ) form of equation (A1) where

$$y + y0 = r\cos\phi \qquad \text{(A6)}$$

and

$$x + x0 = r\sin\phi \qquad \text{(A7)}$$

and where $C = 1$ and $n = m = N$. Thus solving equation (A2) for r, yields

$$r = \left[\frac{(AB)^N}{(A\sin\phi)^N + (B\cos\phi)^N}\right]^{1/N} \qquad \text{(A8)}$$

Therefore, the body Cartesian coordinates may be obtained for $\phi = 0$ to 2π by using equation (A8) and substituting $H/2$ for A, and N may be obtained from expression (A3) to determine r. The Cartesian coordinates Y and Z are then calculated using $Y = r\sin\phi$ and $Z = r\cos\phi + Z0$ where $Z0$ was obtained using expression (A3). As shown in figure A1, the body is divided into four regions and the pylon into two regions with a set of constants for each region.

[1]Taken from reference 9.

TABLE A1. NUMERICAL CONSTANTS FOR FUSELAGE

[From ref. 9]

Function	x/R	C_1	C_2	C_3	C_4	C_5	C_6	C_7	C_8
(a) Fuselage parameters									
H	$0 \rightarrow 0.4$	1.0	−1.0	−0.4	0.4	1.8	0	0.25	1.8
W	↓	1.0	−1.0	−.4	↓	2.0	0	.25	2.0
$Z0$	↓	1.0	−1.0	−.4	↓	1.8	−.08	.08	1.8
N	↓	2.0	3.0	0	↓	1.0	0	1.0	1.0
H	$0.4 \rightarrow 0.8$	.25	0	0	0	0	0	1.0	1.0
W	↓	.25	↓	↓	↓	↓	↓	↓	↓
$Z0$	↓	0	↓	↓	↓	↓	↓	↓	↓
N	↓	5.0	↓	↓	↓	↓	↓	↓	↓
H	$0.8 \rightarrow 1.9$	1.0	−1.0	−.8	1.1	1.5	.05	.2	.6
W	↓	1.0	−1.0	↓	↓	1.5	.05	.2	.6
$Z0$	↓	1.0	−1.0	↓	↓	1.5	.04	−.04	.6
N	↓	5.0	−3.0	↓	↓	1.0	0	1.0	1.0
H	$1.9 \rightarrow 2.0$	1.0	−1.0	−1.9	.1	2.0	0	.05	2.0
W	↓	1.0	−1.0	−1.9	.1	2.0	↓	.05	2.0
$Z0$	↓	.04	0	0	0	0	↓	1.0	1.0
N	↓	2.0	0	0	0	0	↓	1.0	1.0
(b) Pylon parameters									
H	$0.4 \rightarrow 0.8$	1.0	−1.0	−0.8	0.4	3.0	0	0.2	3.0
W	↓	1.0	−1.0	−.8	.4	3.0	↓	.172	3.0
$Z0$	↓	.122	0	0	0	0	↓	1.0	1.0
N	↓	5.0	0	0	0	0	↓	1.0	1.0
H	$0.8 \rightarrow 1.018$	1.0	−1.0	−.8	.218	2.0	0	.2	2.0
W	↓	1.0	−1.0	−.8	.218	2.0	0	.172	2.0
$Z0$	↓	1.0	−1.0	−.8	1.1	1.5	.065	.06	.6
N	↓	.122	0	0	0	0	0	1.0	1.0

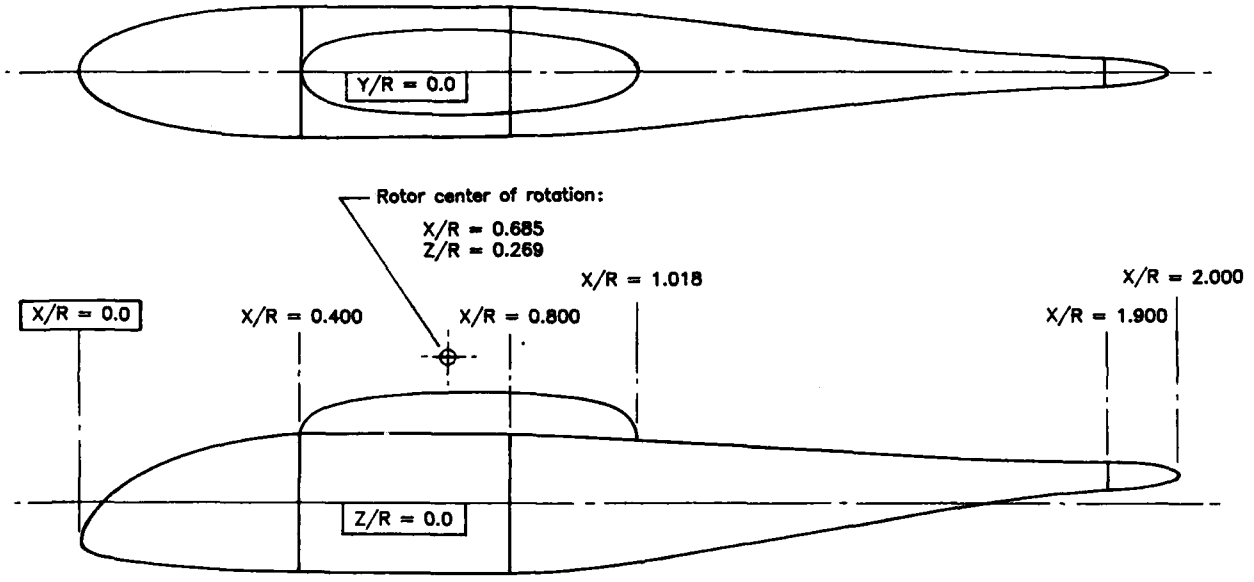

Figure A1. Fuselage component regions (from ref. 9).

References

1. Landgrebe, Anton J.: *An Analytical and Experimental Investigation of Helicopter Rotor Hover Performance and Wake Geometry Characteristics.* USAAMRDL Tech. Rep. 71-24, U.S. Army, June 1971. (Available from DTIC as AD 728 835.)
2. Kocurek, J. David; and Tangler, James L.: A Prescribed Wake Lifting Surface Hover Performance Analysis. *J. American Helicopter Soc.*, vol. 22, no. 1, Jan. 1977, pp. 24–35.
3. Landgrebe, Anton J.; Moffitt, Robert C.; and Clark, David R.: Aerodynamic Technology for Advanced Rotorcraft—Part I. *J. American Helicopter Soc.*, vol. 22, no. 2, Apr. 1977, pp. 21–27.
4. Summa, J. Michael; and Maskew, B.: New Methods for the Calculation of Hover Airloads. Paper No. 15, *Fifth European Rotorcraft and Powered Lift Aircraft Forum* (Amsterdam), Sept. 1979.
5. Kocurek, J. David; Berkowitz, Lenard F.; and Harris, Franklin D.: Hover Performance Methodology at Bell Helicopter Textron. *36th Annual Forum, American Helicopter Soc.*, 1980, pp. 80-3-1–80-3-47. (Available as Preprint No. 80-3.)
6. Summa, J. Michael: Advanced Rotor Analysis Methods for the Aerodynamics of Vortex/Blade Interactions in Hover. Paper No. 2.8, *Eighth European Rotorcraft and Powered Lift Aircraft Forum* (Aix-en-Province, France), Aug.-Sept. 1982.
7. Gessow, Alfred; and Myers, Garry C., Jr.: *Aerodynamics of the Helicopter.* Macmillan Co., c.1952. (Republished 1967 by Frederick Ungar Pub. Co.)
8. Miller, R. H.: *Simplified Free Wake Analyses for Rotors.* ASRL TR 194-3, Dep. Aeronaut. & Astronaut., Massachusetts Inst. of Technol., Aug. 1981.
9. Freeman, Carl E.; and Mineck, Raymond E.: *Fuselage Surface Pressure Measurements of a Helicopter Wind-Tunnel Model With a 3.15-Meter Diameter Single Rotor.* NASA TM-80051, 1979.
10. Van Gaasbeek, J. R.: *Rotorcraft Flight Simulation Computer Program C81, Volume II—User's Manual.* USARTL TR-77-54B, U.S. Army, Oct. 1979.
11. Noonan, Kevin W.; and Bingham, Gene J.: *Aerodynamic Characteristics of Three Helicopter Airfoil Sections at Reynolds Numbers From Model Scale to Full Scale at Mach Numbers From 0.35 to 0.90.* NASA TP-1701, AVRADCOM TR 80-B-5, 1980.

TABLE I. PARAMETRIC DATA FOR BASELINE PLANFORM

V_{tip}	C_T	C_Q	FM
300	0.16008×10^{-2}	0.15441×10^{-3}	0.2933
	$.17625\times10^{-2}$	$.16492\times10^{-3}$	.3173
	$.21516\times10^{-2}$	$.18919\times10^{-3}$	.3730
	$.23488\times10^{-2}$	$.20120\times10^{-3}$	.4000
	$.26589\times10^{-2}$	$.22287\times10^{-3}$	.4350
	$.30701\times10^{-2}$	$.24847\times10^{-3}$	.4841
	$.33093\times10^{-2}$	$.27163\times10^{-3}$	.4956
	$.36260\times10^{-2}$	$.29346\times10^{-3}$	.5261
	$.39770\times10^{-2}$	$.32529\times10^{-3}$	.5452
	$.44154\times10^{-2}$	$.36195\times10^{-3}$	.5732
	$.47349\times10^{-2}$	$.39240\times10^{-3}$	.5871
	$.54147\times10^{-2}$	$.47011\times10^{-3}$	.5993
400	$.18637\times10^{-2}$	$.17377\times10^{-3}$	.3274
	$.21445\times10^{-2}$	$.19928\times10^{-3}$	.3524
	$.24354\times10^{-2}$	$.21503\times10^{-3}$	.3952
	$.24000\times10^{-2}$	$.20710\times10^{-3}$	.4015
	$.28136\times10^{-2}$	$.23375\times10^{-3}$	.4515
	$.32898\times10^{-2}$	$.25184\times10^{-3}$	.5298
	$.35306\times10^{-2}$	$.28701\times10^{-3}$	.5169
	$.39180\times10^{-2}$	$.31577\times10^{-3}$	.5492
	$.42516\times10^{-2}$	$.34013\times10^{-3}$	.5763
	$.47332\times10^{-2}$	$.37702\times10^{-3}$	.6107
	$.49035\times10^{-2}$	$.41615\times10^{-3}$	.5834
	$.53570\times10^{-2}$	$.45525\times10^{-3}$	.6090
	$.56732\times10^{-2}$	$.48215\times10^{-3}$	.6267
500	$.16964\times10^{-2}$	$.15867\times10^{-3}$	.3114
	$.20213\times10^{-2}$	$.18057\times10^{-3}$	.3559
	$.23177\times10^{-2}$	$.19816\times10^{-3}$	.3982
	$.26309\times10^{-2}$	$.21679\times10^{-3}$	.4402
	$.30221\times10^{-2}$	$.24408\times10^{-3}$	.4813
	$.34732\times10^{-2}$	$.27780\times10^{-3}$	.5210
	$.38007\times10^{-2}$	$.30276\times10^{-3}$	.5473
	$.41839\times10^{-2}$	$.33566\times10^{-3}$	.5701
	$.45458\times10^{-2}$	$.36957\times10^{-3}$	.5864
	$.49634\times10^{-2}$	$.40736\times10^{-3}$	.6070
	$.53726\times10^{-2}$	$.44773\times10^{-3}$	.6219
	$.57316\times10^{-2}$	$.48943\times10^{-3}$	.6269
	$.59317\times10^{-2}$	$.50544\times10^{-3}$	.6391
600	$.17916\times10^{-2}$	$.16492\times10^{-3}$	.3251
	$.21813\times10^{-2}$	$.18785\times10^{-3}$	.3835
	$.25526\times10^{-2}$	$.21144\times10^{-3}$	.4313
	$.28685\times10^{-2}$	$.23909\times10^{-3}$	.4544
	$.32268\times10^{-2}$	$.26410\times10^{-3}$	.4908
	$.36959\times10^{-2}$	$.29198\times10^{-3}$	.5442
	$.40301\times10^{-2}$	$.32436\times10^{-3}$	.5578
	$.44156\times10^{-2}$	$.35853\times10^{-3}$	.5787
	$.47727\times10^{-2}$	$.38998\times10^{-3}$	.5979
	$.52020\times10^{-2}$	$.42918\times10^{-3}$	.6182
	$.55926\times10^{-2}$	$.47113\times10^{-3}$	.6277
	$.59775\times10^{-2}$	$.52013\times10^{-3}$	.6283
	$.61836\times10^{-2}$	$.53203\times10^{-3}$	.6463

TABLE II. PARAMETRIC DATA FOR TR3 PLANFORM

V_{tip}	C_T	C_Q	FM
300	0.18497×10^{-2}	0.16889×10^{-3}	0.3331
	$.21285\times10^{-2}$	$.18304\times10^{-3}$	.3794
	$.24738\times10^{-2}$	$.20716\times10^{-3}$	.4200
	$.26948\times10^{-2}$	$.22755\times10^{-3}$	.4347
	$.31549\times10^{-2}$	$.25761\times10^{-3}$	.4864
	$.34756\times10^{-2}$	$.28495\times10^{-3}$	.5085
	$.37369\times10^{-2}$	$.30901\times10^{-3}$	.5227
	$.42115\times10^{-2}$	$.34403\times10^{-3}$	.5617
	$.45219\times10^{-2}$	$.37849\times10^{-3}$	.5681
	$.47681\times10^{-2}$	$.40330\times10^{-3}$	.5773
	$.52475\times10^{-2}$	$.44064\times10^{-3}$	.6100
	$.57528\times10^{-2}$	$.49837\times10^{-3}$	.6191
	$.56924\times10^{-2}$	$.49509\times10^{-3}$	.6134
400	$.20688\times10^{-2}$	$.16950\times10^{-3}$	.3920
	$.25110\times10^{-2}$	$.19910\times10^{-3}$	.4469
	$.28789\times10^{-2}$	$.22424\times10^{-3}$	.4871
	$.31262\times10^{-2}$	$.24590\times10^{-3}$	.5026
	$.35762\times10^{-2}$	$.27643\times10^{-3}$	.5471
	$.39693\times10^{-2}$	$.30362\times10^{-3}$	.5824
	$.43427\times10^{-2}$	$.33839\times10^{-3}$	.5980
	$.48247\times10^{-2}$	$.37636\times10^{-3}$	.6296
	$.51304\times10^{-2}$	$.40146\times10^{-3}$	.6473
	$.55067\times10^{-2}$	$.44283\times10^{-3}$	.6525
	$.58969\times10^{-2}$	$.48250\times10^{-3}$	.6636
	$.62145\times10^{-2}$	$.51466\times10^{-3}$	.6731
	$.65625\times10^{-2}$	$.55281\times10^{-3}$	.6800
	$.70391\times10^{-2}$	$.60406\times10^{-3}$	.6913
	$.74137\times10^{-2}$	$.64561\times10^{-3}$	.6991
500	$.77677\times10^{-3}$	$.11545\times10^{-3}$	.1326
	$.11000\times10^{-2}$	$.12673\times10^{-3}$	.2036
	$.13739\times10^{-2}$	$.13919\times10^{-3}$	.2587
	$.16814\times10^{-2}$	$.15317\times10^{-3}$	.3183
	$.19997\times10^{-2}$	$.16908\times10^{-3}$	.3740
	$.22922\times10^{-2}$	$.18498\times10^{-3}$	.4195
	$.26562\times10^{-2}$	$.20831\times10^{-3}$	.4647
	$.30054\times10^{-2}$	$.23234\times10^{-3}$	.5014
	$.33066\times10^{-2}$	$.25482\times10^{-3}$	.5276
	$.37267\times10^{-2}$	$.28463\times10^{-3}$	.5652
	$.40353\times10^{-2}$	$.30806\times10^{-3}$	.5884
	$.44991\times10^{-2}$	$.34899\times10^{-3}$	.6115
	$.48907\times10^{-2}$	$.38054\times10^{-3}$	.6355
	$.52060\times10^{-2}$	$.40857\times10^{-3}$	.6501
	$.56003\times10^{-2}$	$.44771\times10^{-3}$	.6619
	$.59650\times10^{-2}$	$.48211\times10^{-3}$	.6757
	$.63444\times10^{-2}$	$.52308\times10^{-3}$	.6831
	$.66774\times10^{-2}$	$.55858\times10^{-3}$	.6907
	$.71108\times10^{-2}$	$.61019\times10^{-3}$	.6949
	$.74862\times10^{-2}$	$.65596\times10^{-3}$	.6982
600	$.48444\times10^{-3}$	$.10845\times10^{-3}$	.0695
	$.11171\times10^{-2}$	$.12925\times10^{-3}$	.2043
	$.17189\times10^{-2}$	$.15578\times10^{-3}$	.3235
	$.23135\times10^{-2}$	$.19142\times10^{-3}$	.4111
	$.32223\times10^{-2}$	$.25264\times10^{-3}$	.5119
	$.39600\times10^{-2}$	$.30498\times10^{-3}$	.5778
	$.41344\times10^{-2}$	$.31261\times10^{-3}$	.6013
	$.46433\times10^{-2}$	$.36146\times10^{-3}$	.6190
	$.54358\times10^{-2}$	$.42533\times10^{-3}$	.6663
	$.61230\times10^{-2}$	$.49584\times10^{-3}$	.6833
	$.64964\times10^{-2}$	$.53697\times10^{-3}$	.6895
	$.68631\times10^{-2}$	$.57631\times10^{-3}$	.6976
	$.72616\times10^{-2}$	$.62600\times10^{-3}$	.6990

TABLE III. PARAMETRIC DATA FOR TR5 PLANFORM

V_{tip}	C_T	C_Q	FM
300	0.16554×10^{-2}	0.16036×10^{-3}	0.2970
↓	$.16465\times10^{-2}$	$.15349\times10^{-3}$	.3078
	$.24119\times10^{-2}$	$.19684\times10^{-3}$	.4255
	$.32202\times10^{-2}$	$.25844\times10^{-3}$	.5000
	$.38767\times10^{-2}$	$.31548\times10^{-3}$	.5410
	$.46371\times10^{-2}$	$.36897\times10^{-3}$	.6051
	$.53690\times10^{-2}$	$.44203\times10^{-3}$	.6293
	$.57318\times10^{-2}$	$.48352\times10^{-3}$	.6346
	$.60987\times10^{-2}$	$.51880\times10^{-3}$	.6491
	$.65462\times10^{-2}$	$.57476\times10^{-3}$	.6516
	$.66482\times10^{-2}$	$.58635\times10^{-3}$	.6534
	$.72548\times10^{-2}$	$.64946\times10^{-3}$	.6728
400	$.16609\times10^{-2}$	$.14573\times10^{-3}$	.3284
↓	$.23676\times10^{-2}$	$.19333\times10^{-3}$	.4214
	$.30618\times10^{-2}$	$.24206\times10^{-3}$	.4949
	$.37391\times10^{-2}$	$.29303\times10^{-3}$	.5518
	$.44462\times10^{-2}$	$.35529\times10^{-3}$	.5901
	$.51444\times10^{-2}$	$.42290\times10^{-3}$	.6170
	$.54188\times10^{-2}$	$.45310\times10^{-3}$	.6225
	$.58132\times10^{-2}$	$.48639\times10^{-3}$	.6444
	$.61300\times10^{-2}$	$.52266\times10^{-3}$	.6493
	$.64175\times10^{-2}$	$.55863\times10^{-3}$	.6508
	$.67429\times10^{-2}$	$.59466\times10^{-3}$	.6584
500	$.21289\times10^{-3}$	$.93150\times10^{-4}$	.0236
↓	$.16265\times10^{-3}$	$.89885\times10^{-4}$	.0163
	$.67187\times10^{-3}$	$.99983\times10^{-4}$	.1232
	$.12840\times10^{-2}$	$.12585\times10^{-3}$	.2585
	$.17337\times10^{-2}$	$.14754\times10^{-3}$	.3460
	$.26254\times10^{-2}$	$.20202\times10^{-3}$	.4709
	$.32327\times10^{-2}$	$.24890\times10^{-3}$	.5222
	$.38721\times10^{-2}$	$.29801\times10^{-3}$	.5717
	$.46239\times10^{-2}$	$.36016\times10^{-3}$	.6173
	$.52689\times10^{-2}$	$.41820\times10^{-3}$	.6467
	$.55445\times10^{-2}$	$.45151\times10^{-3}$	.6466
	$.57940\times10^{-2}$	$.48187\times10^{-3}$	.6472
	$.61801\times10^{-2}$	$.51292\times10^{-3}$	.6698
	$.65515\times10^{-2}$	$.55998\times10^{-3}$	.6696
	$.68682\times10^{-2}$	$.59887\times10^{-3}$	.6721
600	$.23202\times10^{-3}$	$.98475\times10^{-4}$	.0254
↓	$.14573\times10^{-3}$	$.85009\times10^{-4}$	.0146
	$.74313\times10^{-3}$	$.10076\times10^{-3}$	.1422
	$.13198\times10^{-2}$	$.12546\times10^{-3}$	.2703
	$.19856\times10^{-2}$	$.16351\times10^{-3}$	.3827
	$.27473\times10^{-2}$	$.21347\times10^{-3}$	.4770
	$.33660\times10^{-2}$	$.25763\times10^{-3}$	.5346
	$.40520\times10^{-2}$	$.31099\times10^{-3}$	.5865
	$.46667\times10^{-2}$	$.36010\times10^{-3}$	.6260
	$.53304\times10^{-2}$	$.43277\times10^{-3}$	.6359
	$.56930\times10^{-2}$	$.46533\times10^{-3}$	.6527
	$.59786\times10^{-2}$	$.49603\times10^{-3}$	.6590
	$.64211\times10^{-2}$	$.54805\times10^{-3}$	.6639
	$.68343\times10^{-2}$	$.59290\times10^{-3}$	.6738

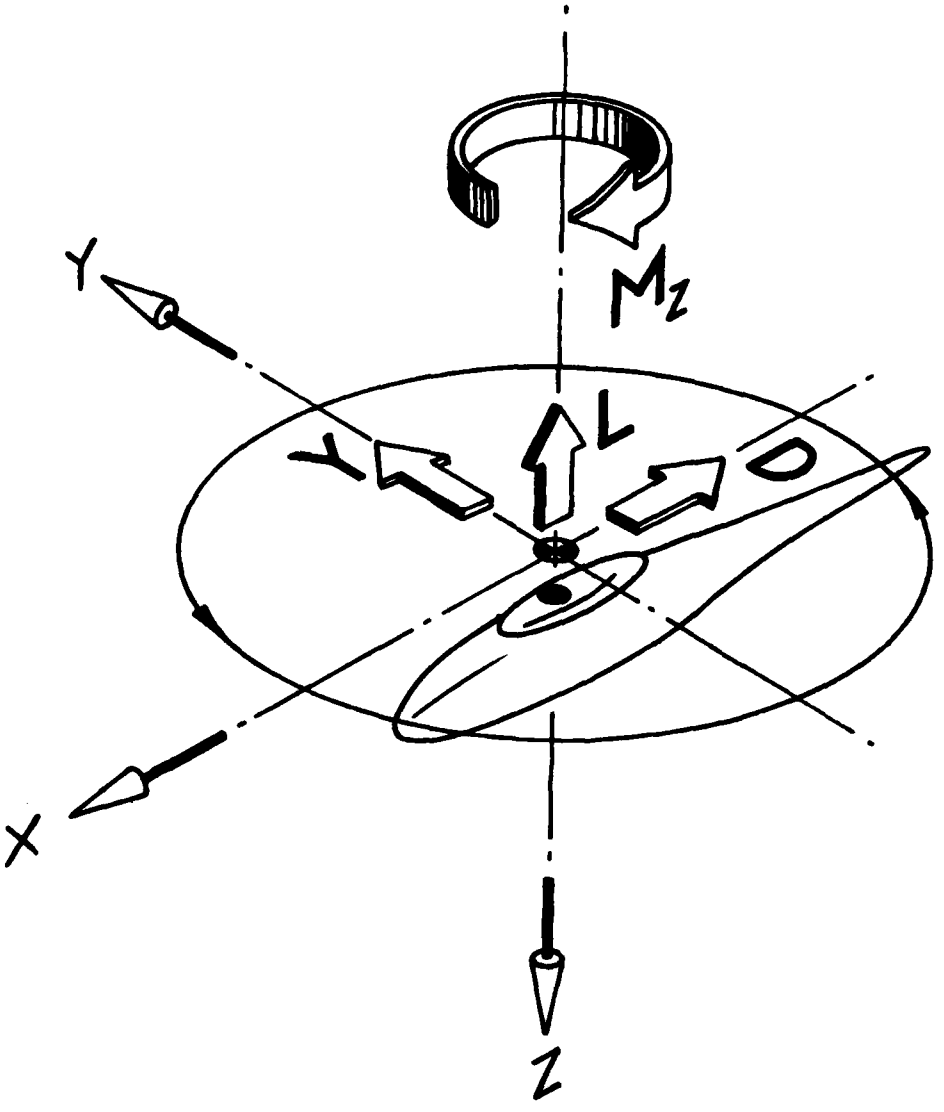

Figure 1. Axis system used in presentation of data. Arrows denote positive directions of axes, forces, and moments.

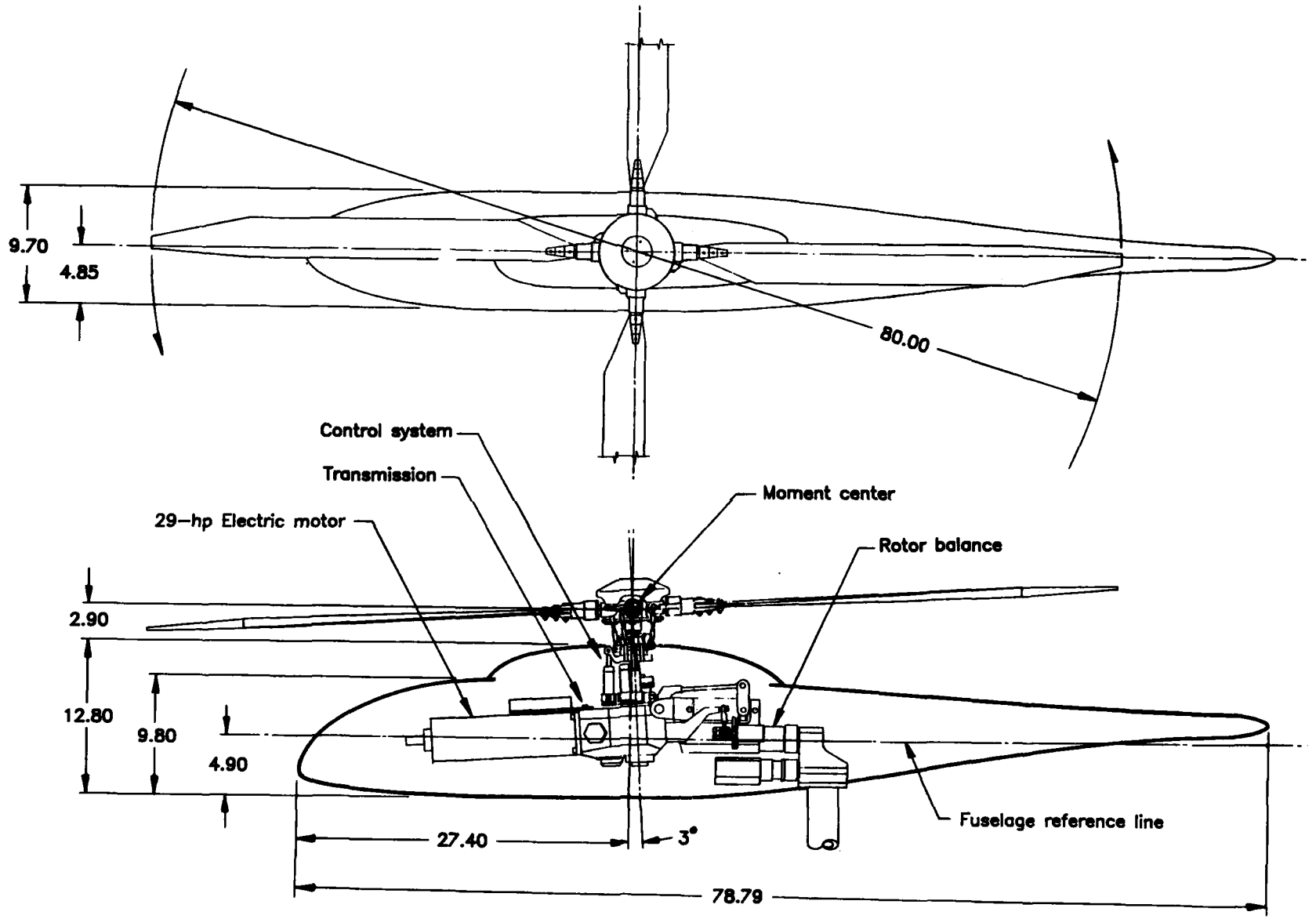

(a) General arrangement. Linear dimensions are in inches.

Figure 2. Details of model used in investigation.

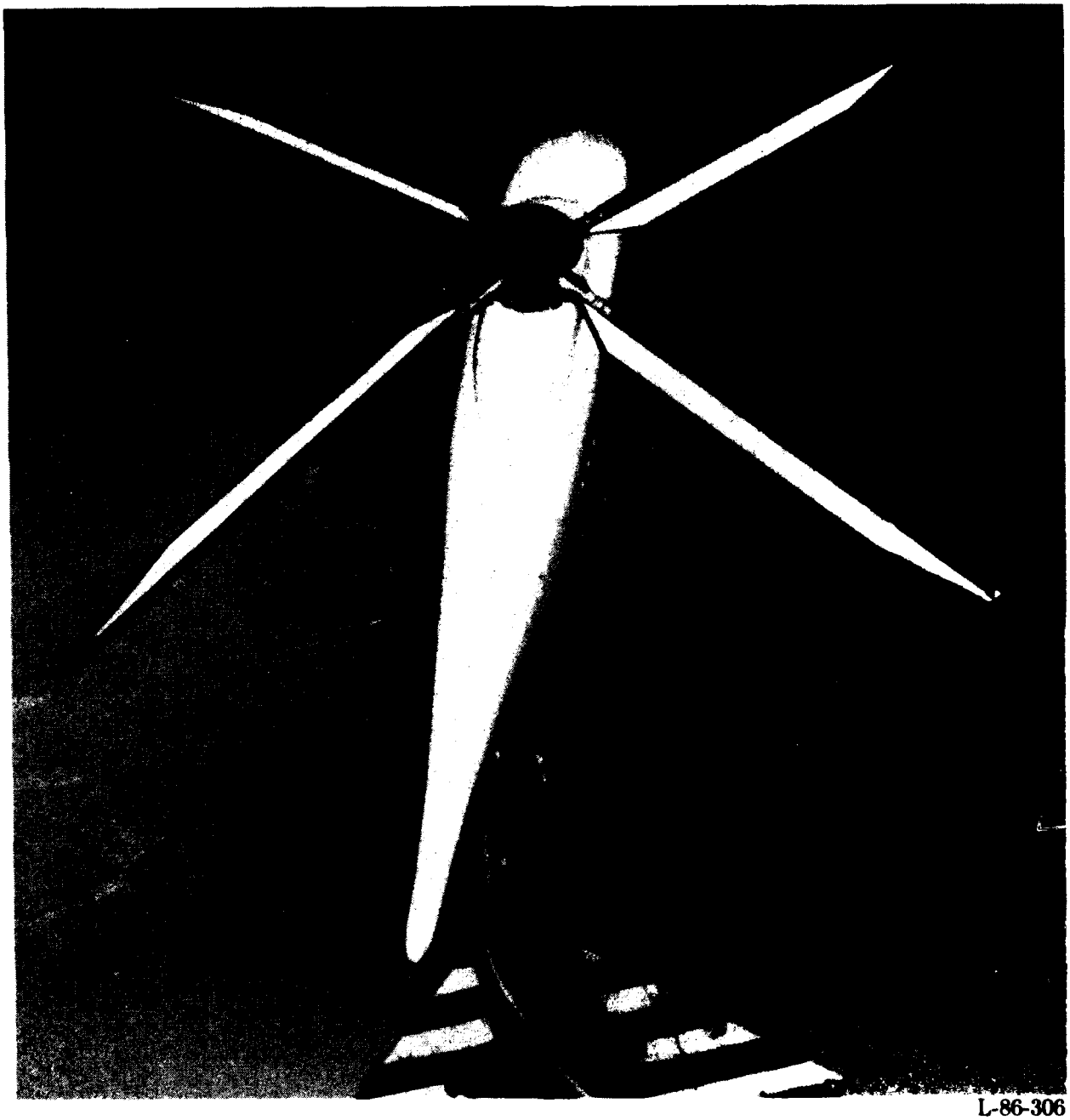

L-86-306

(b) TR3 blades mounted for hover testing on 2-m rotor test rig.

Figure 2. Concluded.

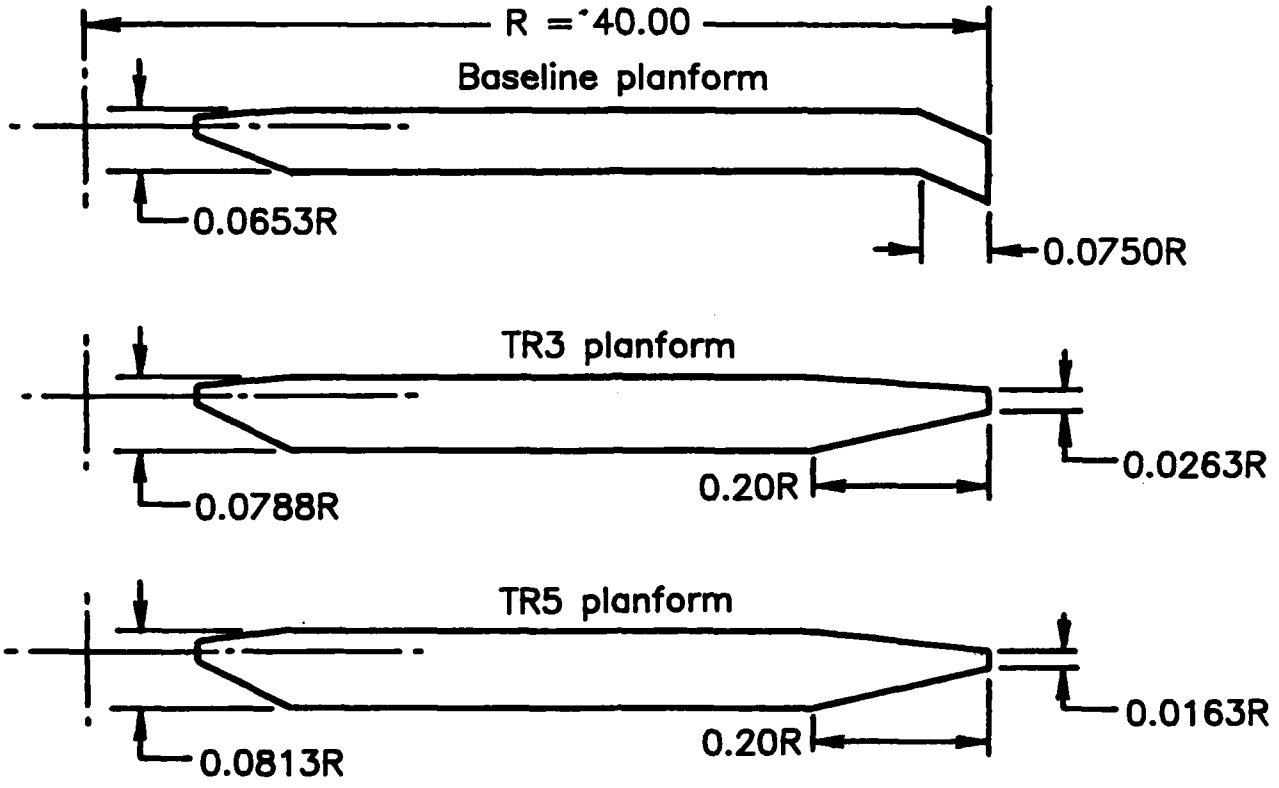

Planform	Twist, deg (See fig. 3(b))	Taper ratio	Tip sweep, deg
Baseline	−16 (nonlinear)	1:1	20 (aft)
TR3	−16	3:1	0
TR5	−16	5:1	0

(a) Blade planform details. NACA 0012 airfoil section used for all blades. $\sigma_T = 0.0825$.

Figure 3. Rotor blades used in investigation. Linear dimensions are in inches.

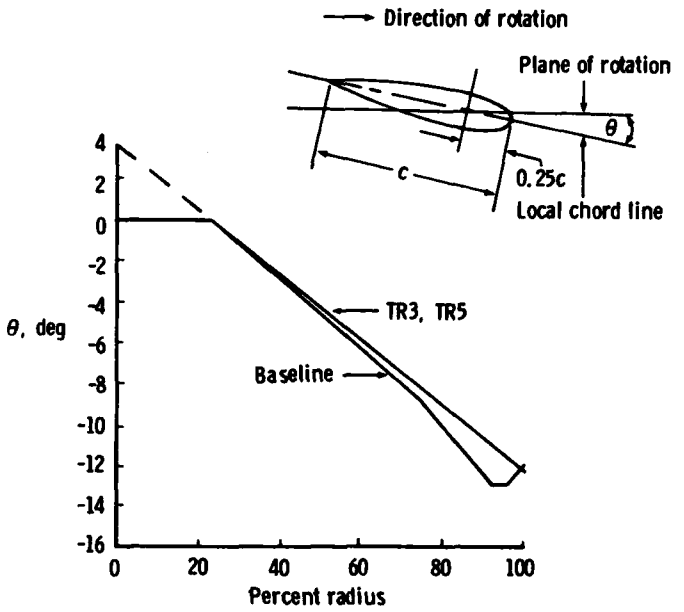

(b) Blade twist distribution.

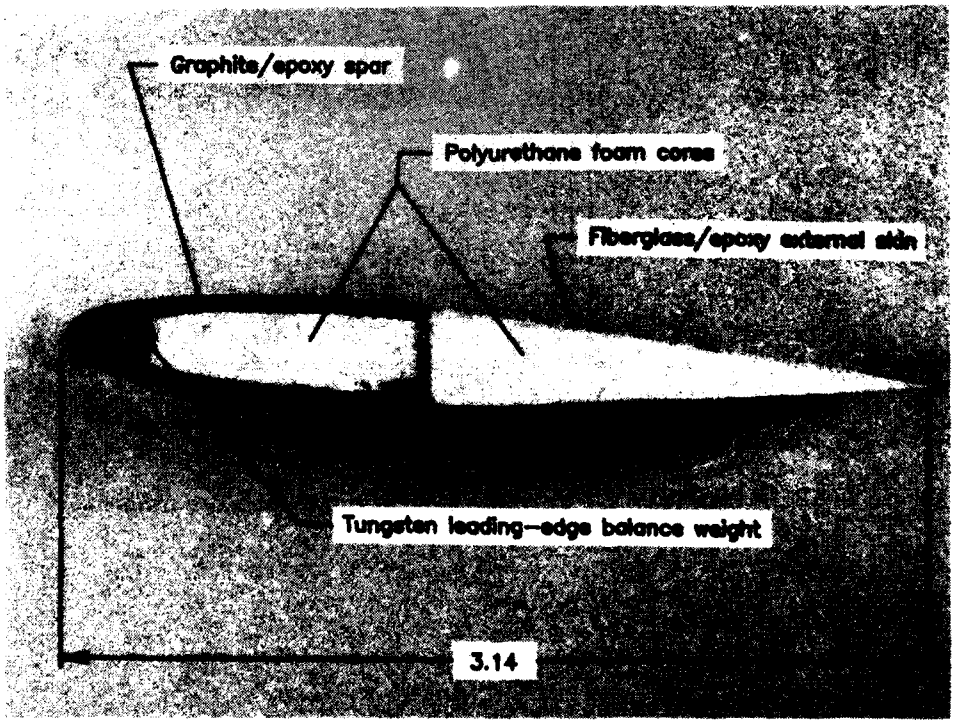

L-86-307

(c) Details of model rotor blade construction for TR3 planform.

Figure 3. Concluded.

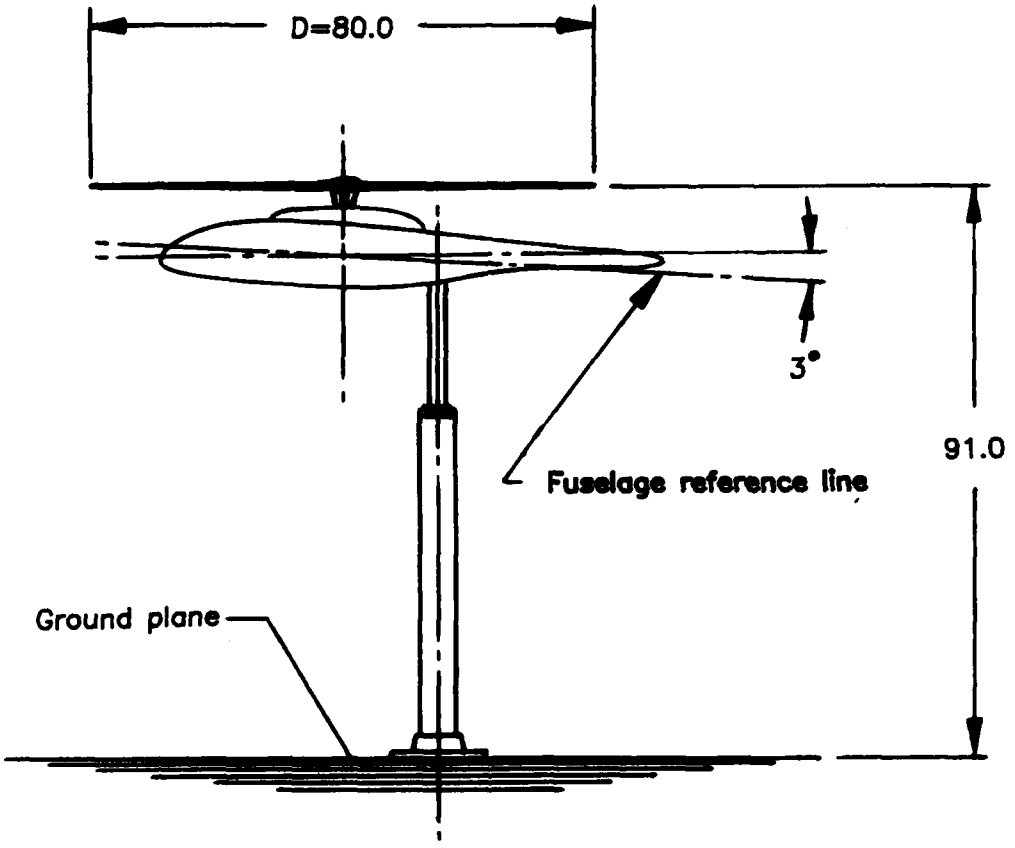

Figure 4. Model mounting arrangement. Linear dimensions are in inches.

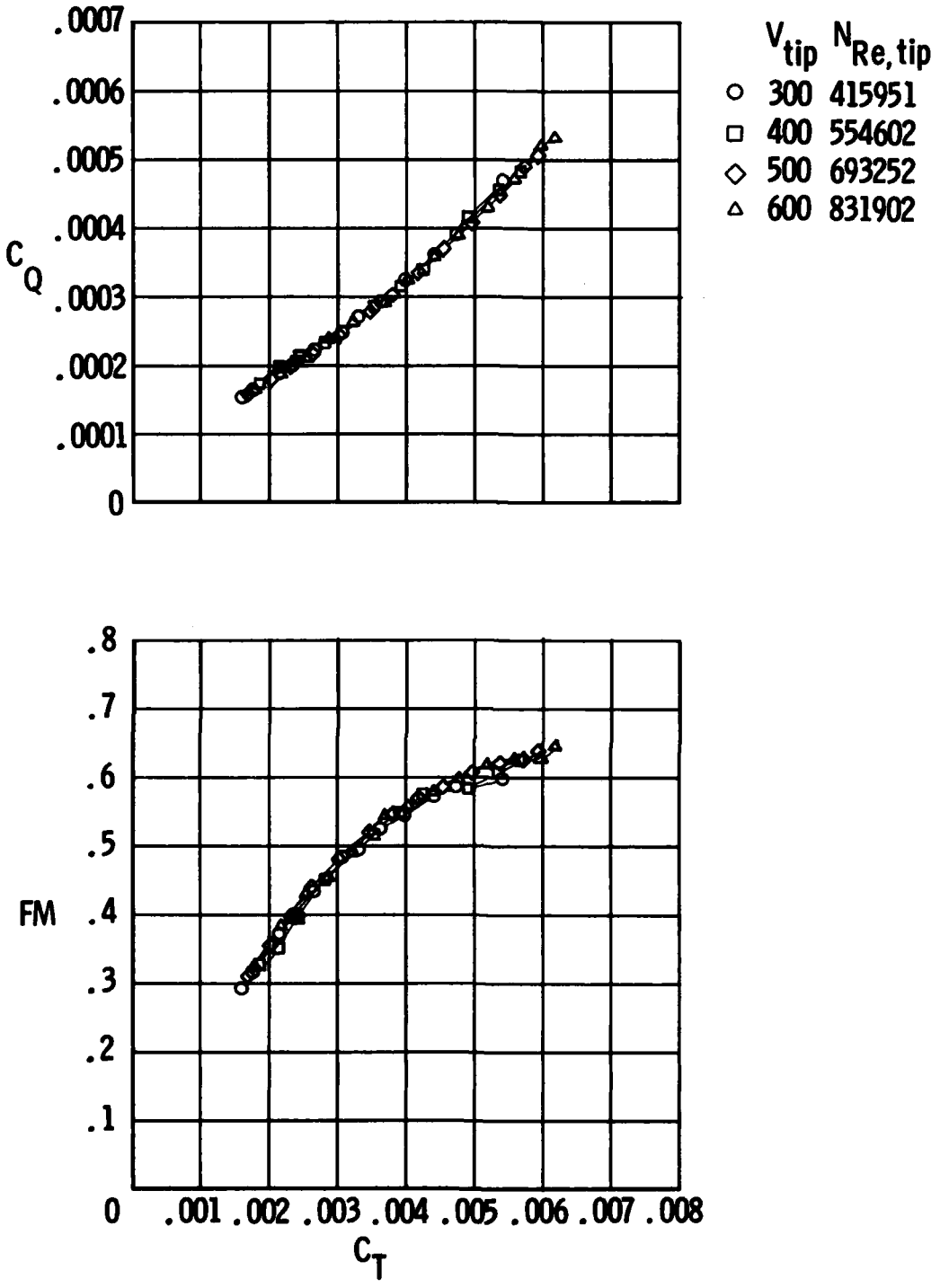

(a) Baseline planform.

Figure 5. Basic aerodynamic characteristics of rotors.

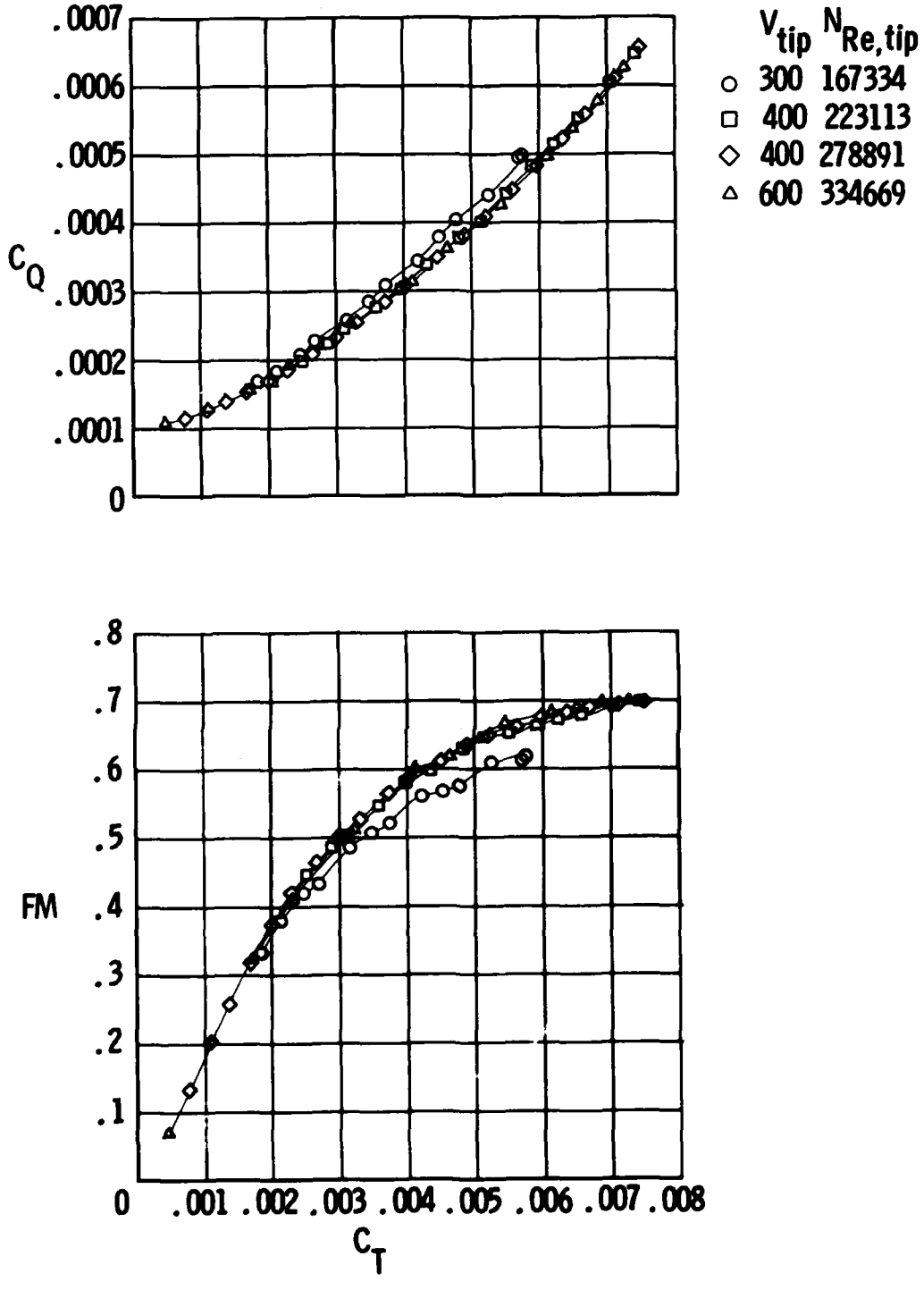

(b) TR3 planform.

Figure 5. Continued.

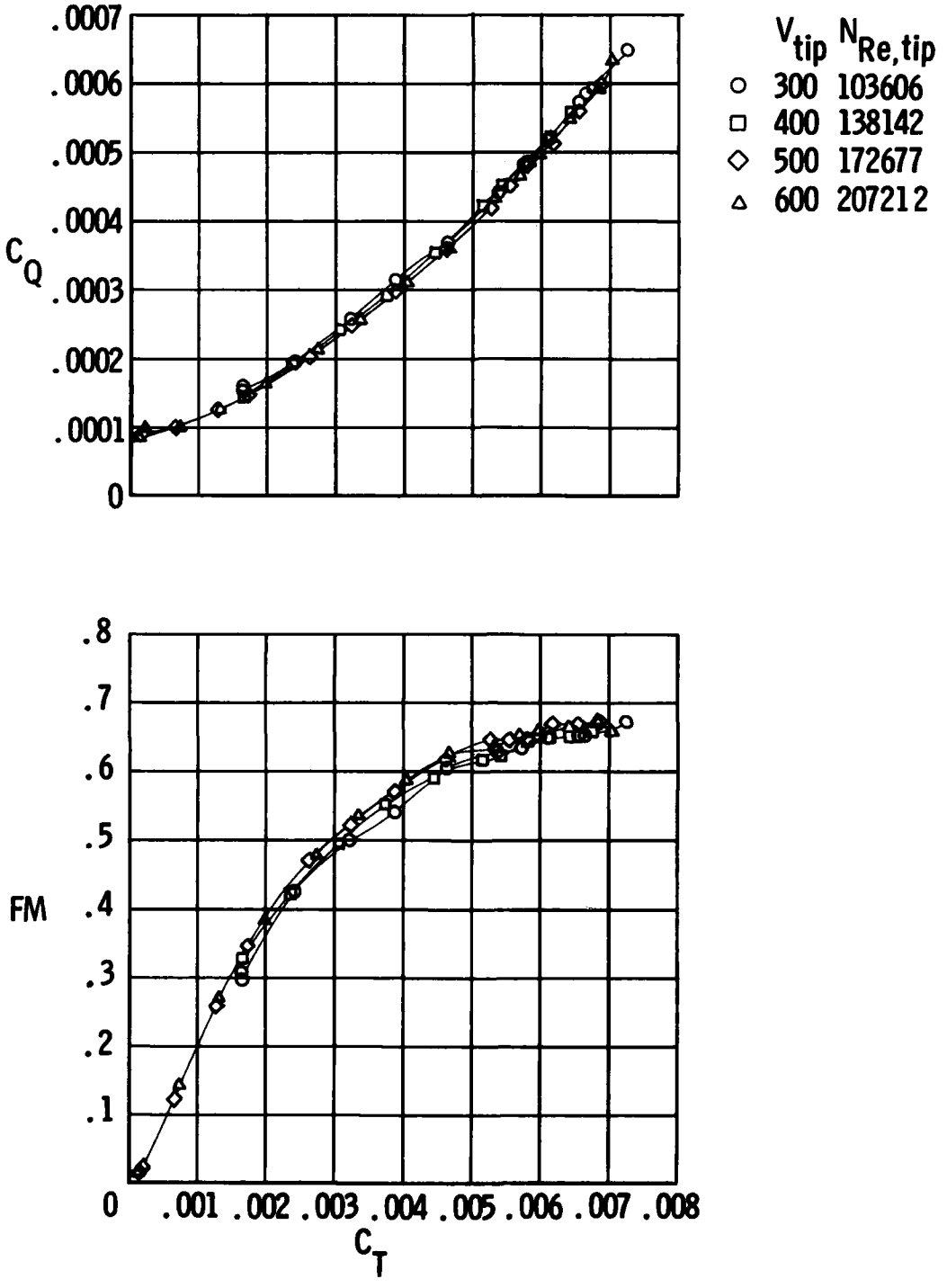

(c) TR5 planform.

Figure 5. Concluded.

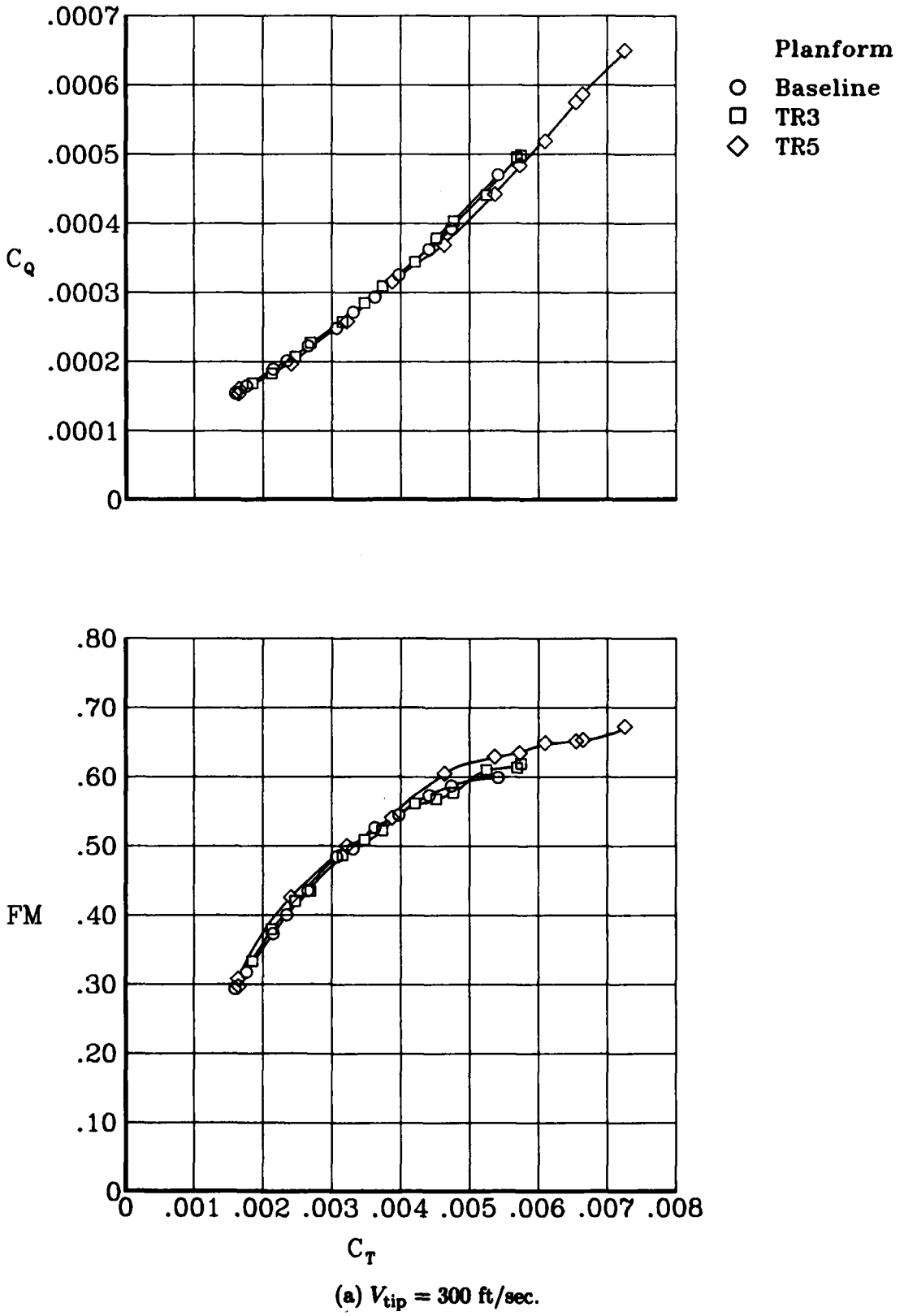

(a) $V_{tip} = 300$ ft/sec.

Figure 6. Comparison of aerodynamic characteristics of three rotors at two tip speeds.

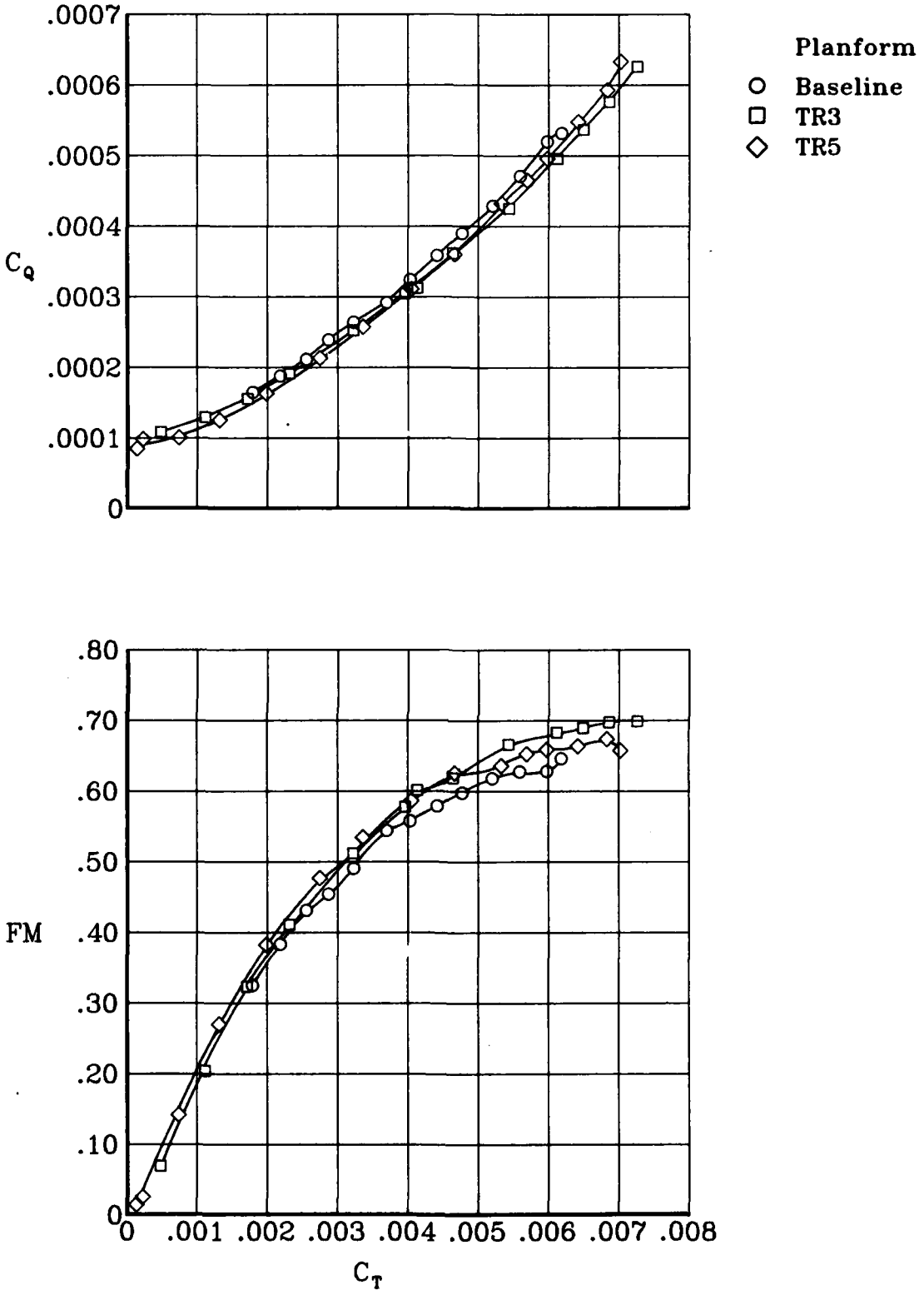

(b) $V_{tip} = 600$ ft/sec.

Figure 6. Concluded.

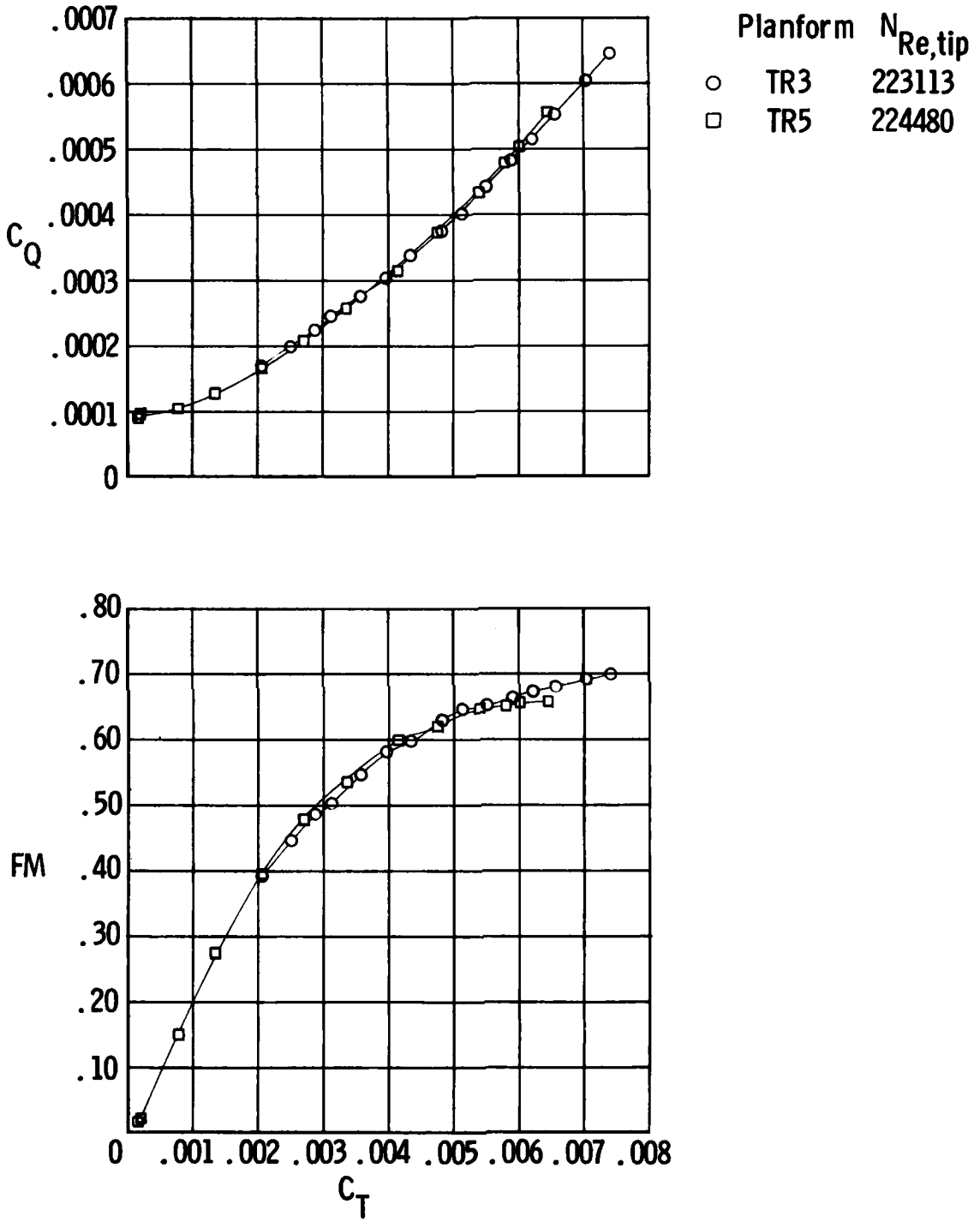

Figure 7. Comparison of aerodynamic characteristics of TR3 and TR5 rotors operating at approximately the same tip Reynolds number.

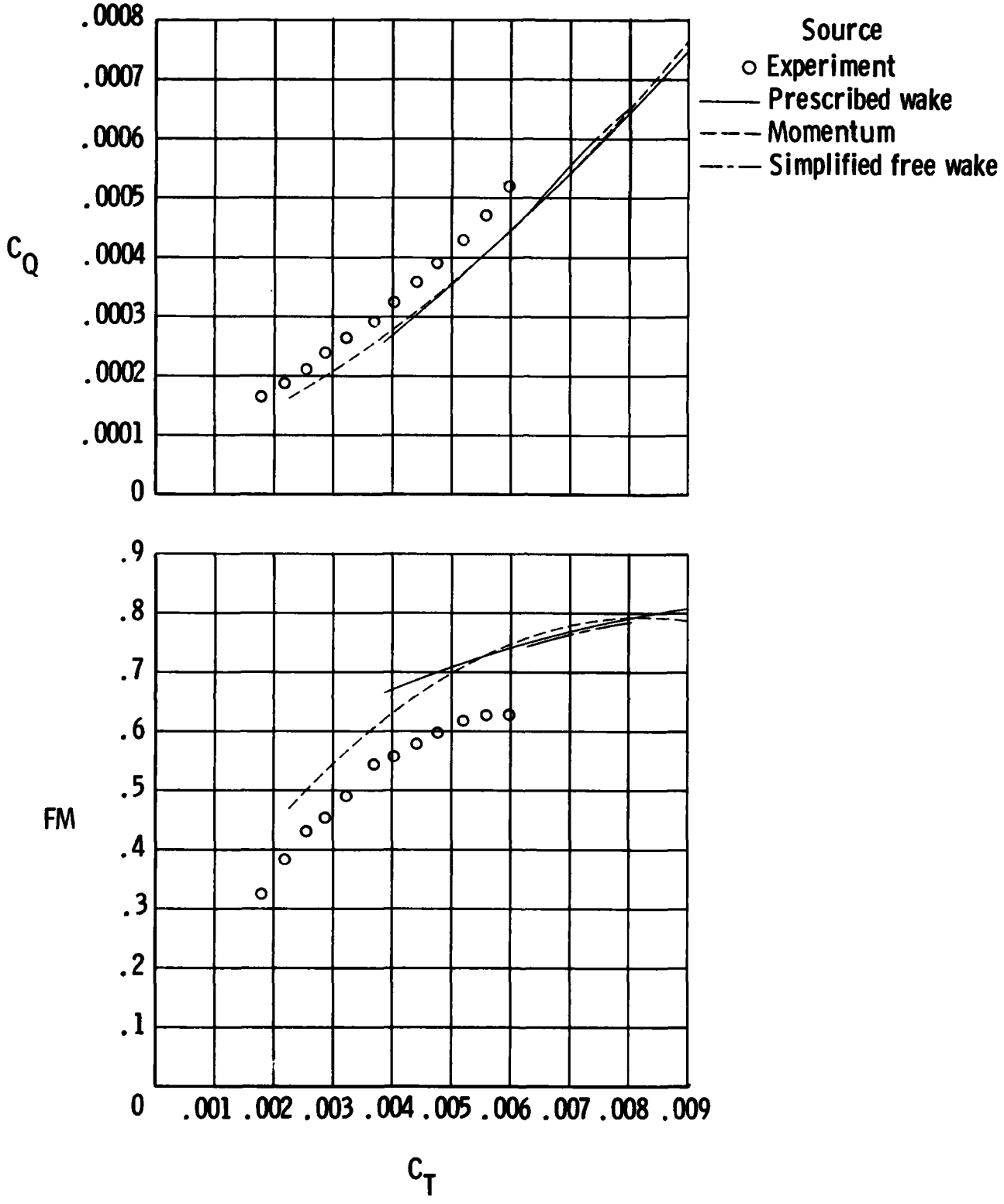

(a) Baseline planform.

Figure 8. Comparison of test data with predictions from three analyses. V_{tip} = 600 ft/sec for experimental data.

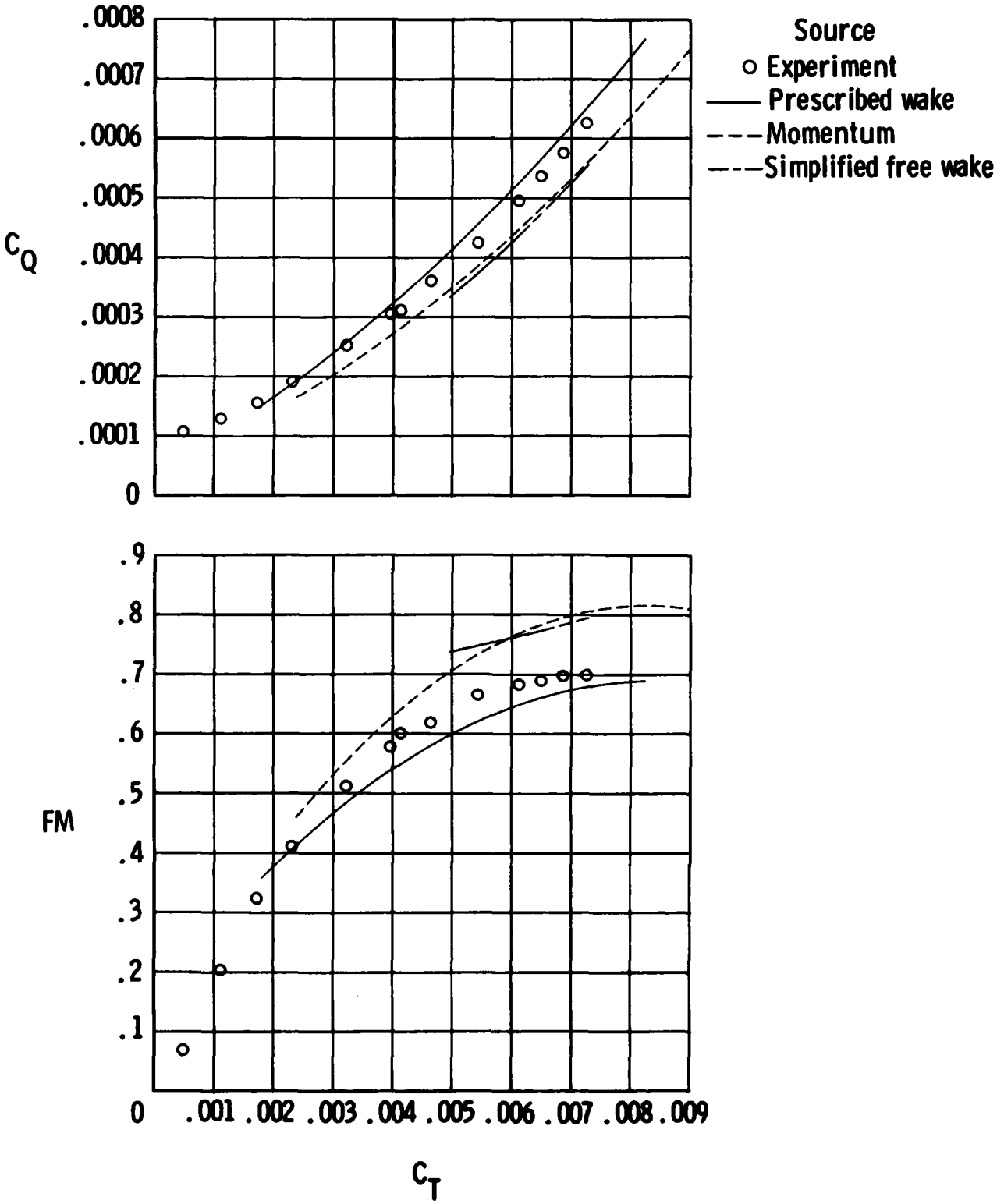

(b) TR3 planform.

Figure 8. Continued.

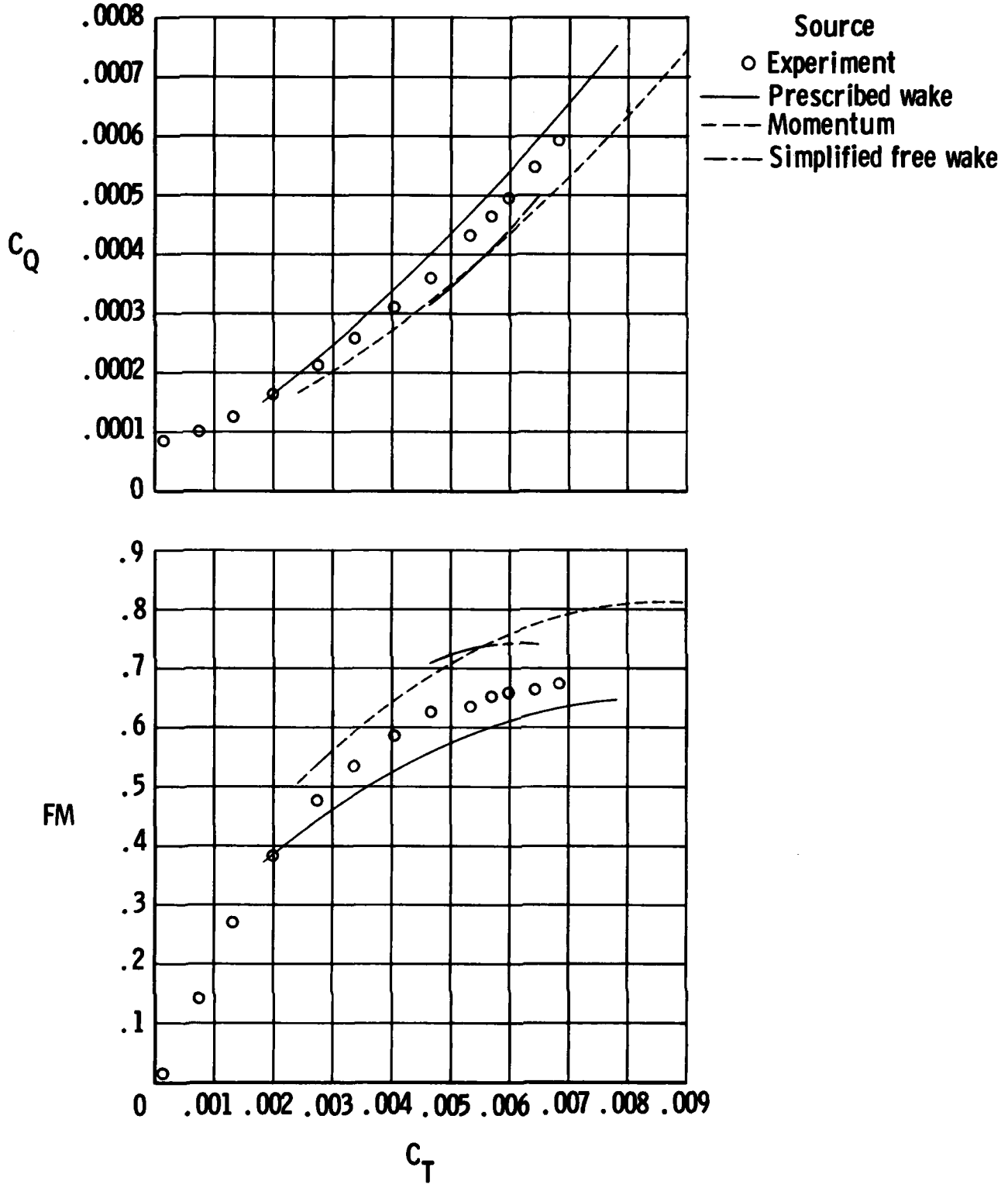

(c) TR5 planform.

Figure 8. Concluded.

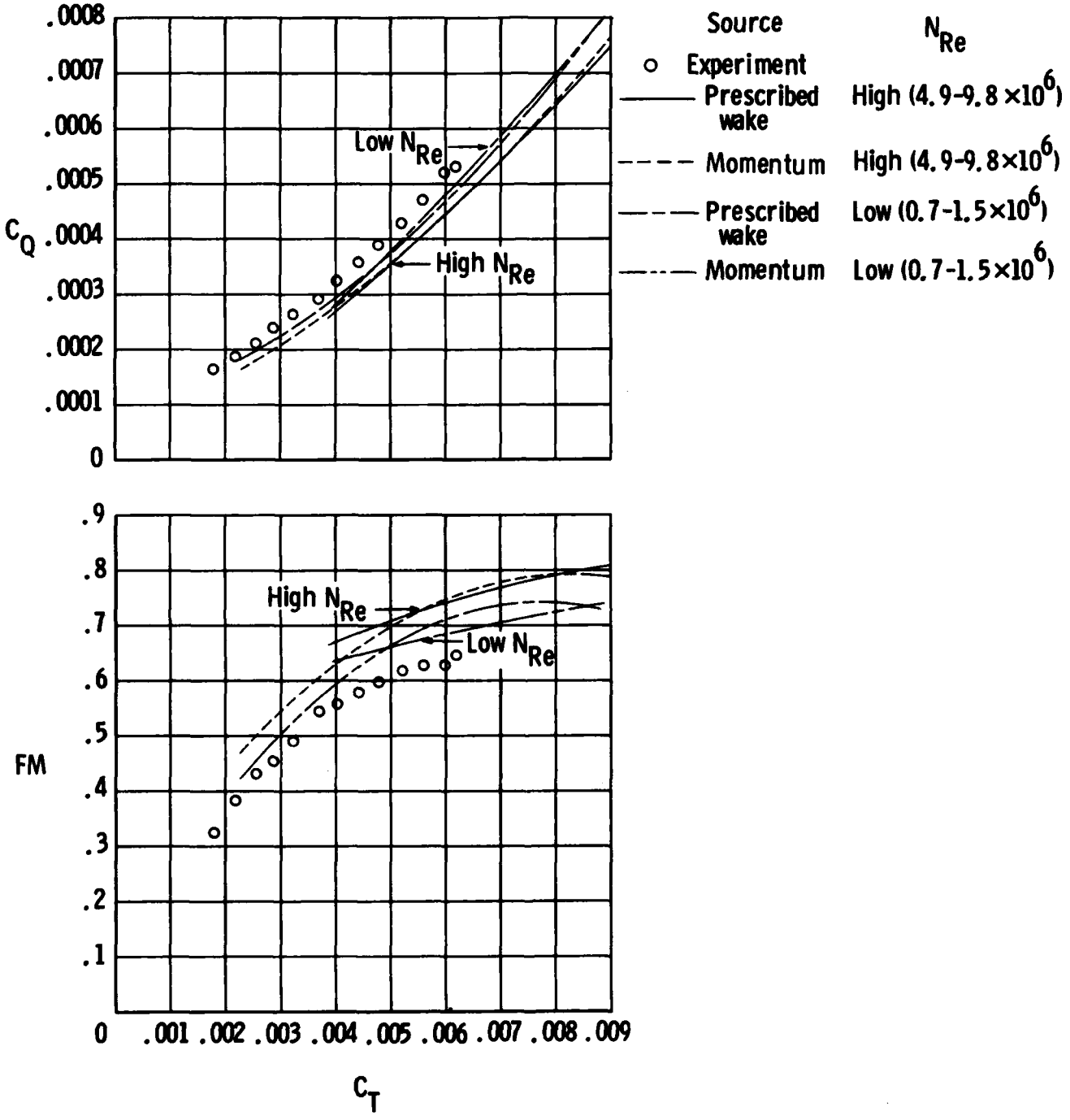

(a) Baseline planform.

Figure 9. Effect of Reynolds number on prescribed-wake and momentum analyses. V_{tip} = 600 ft/sec for experimental data.

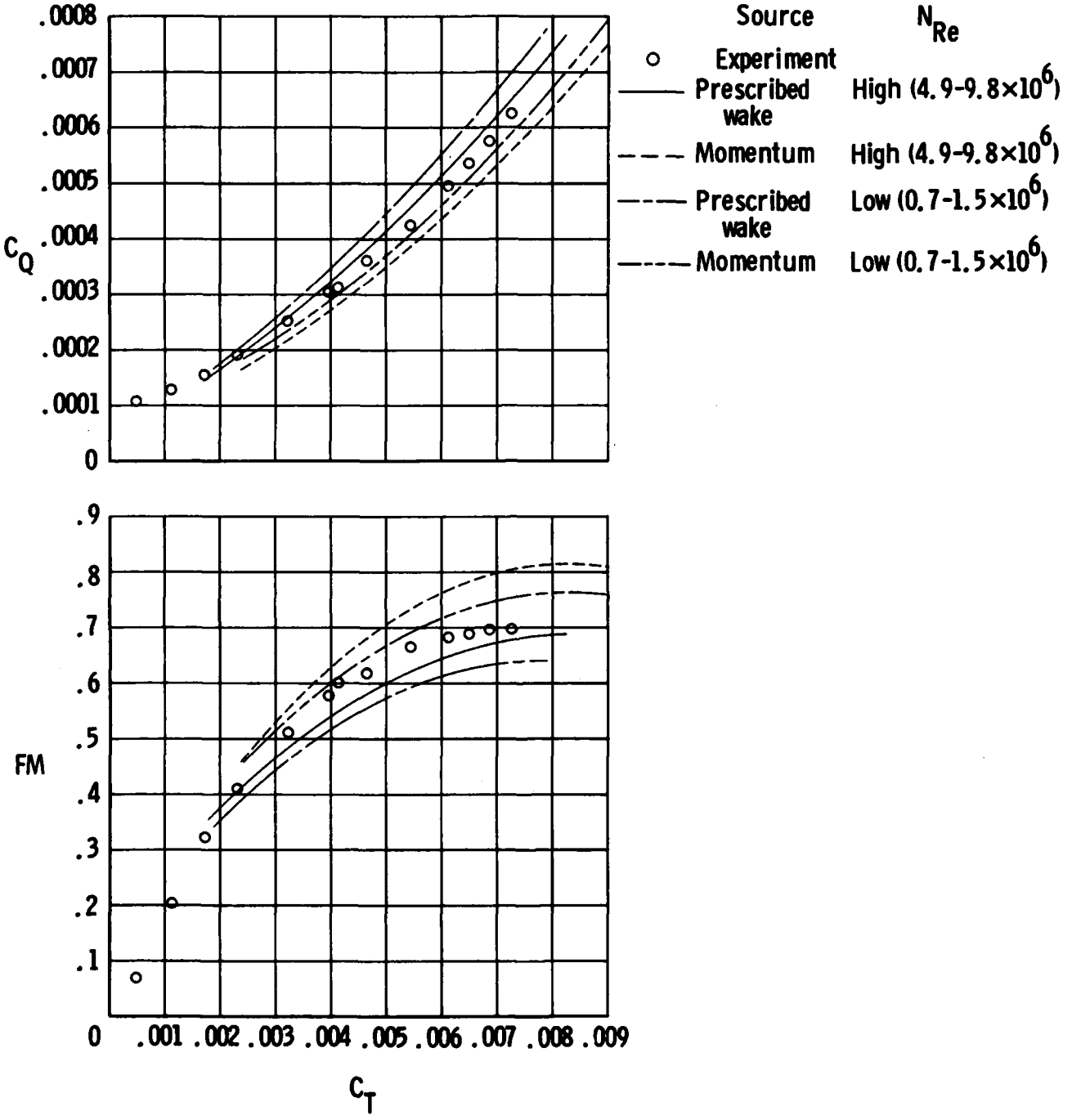

(b) TR3 planform.

Figure 9. Continued.

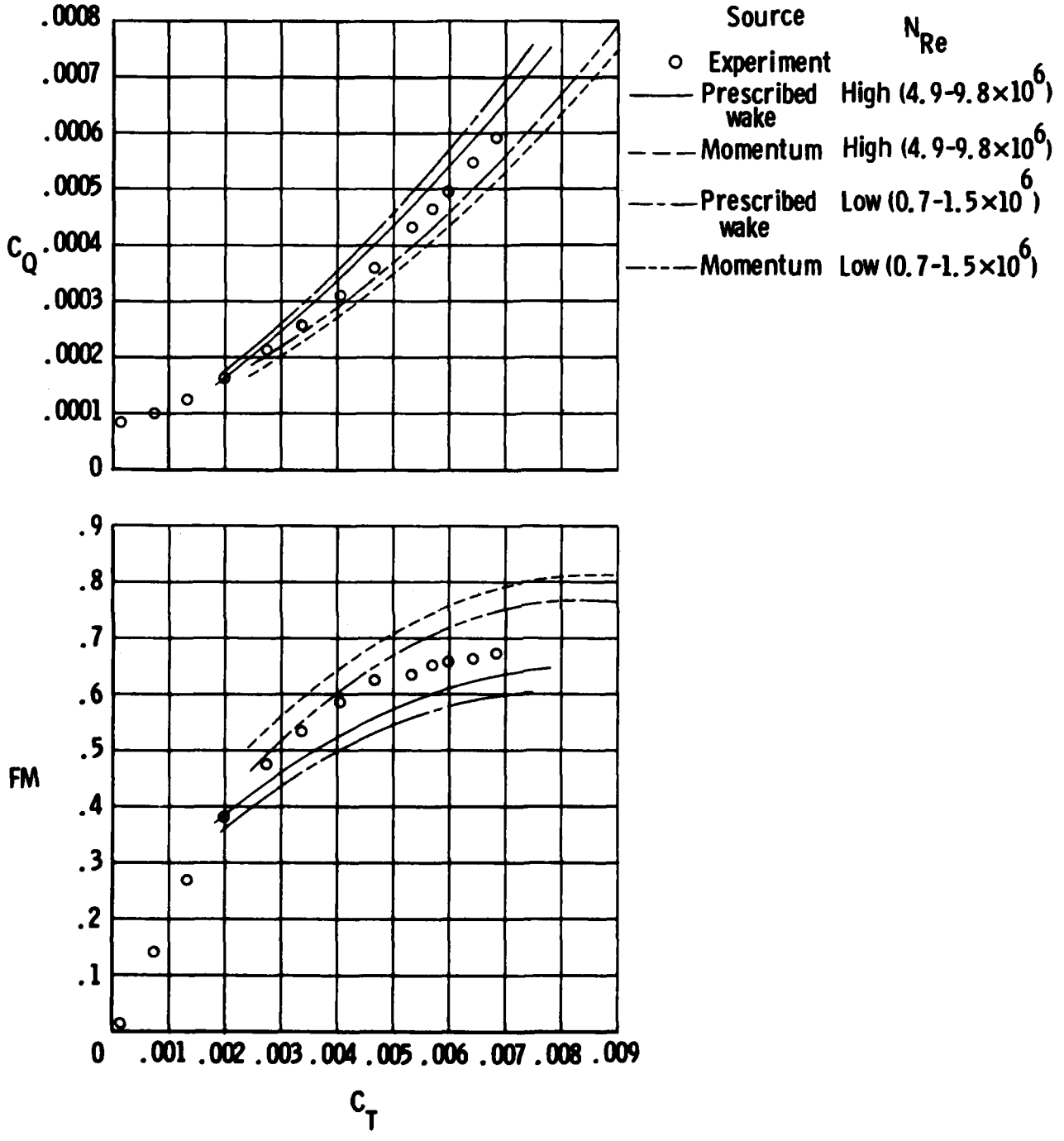

(c) TR5 planform.

Figure 9. Concluded.

END

DTIC

5-86